University Library

MINERVA ACCESS

A gateway to Melbourne's research publications

Minerva Access is the Institutional Repository of The University of Melbourne

Author/s:
Giannangelo, C;Siddiqui, G;de Paoli, A;Anderson, BM;Edgington-Mitchell, LE;Charman, SA;Creek, DJ

Title:
System-wide biochemical analysis reveals ozonide antimalarials initially act by disrupting Plasmodium falciparum haemoglobin digestion

Date:
2020-06-01

Citation:
Giannangelo, C., Siddiqui, G., de Paoli, A., Anderson, B. M., Edgington-Mitchell, L. E., Charman, S. A. & Creek, D. J. (2020). System-wide biochemical analysis reveals ozonide antimalarials initially act by disrupting Plasmodium falciparum haemoglobin digestion. Plos Pathogens, 16 (6), https://doi.org/10.1371/journal.ppat.1008485.

Persistent Link:
https://hdl.handle.net/11343/244517

License:
CC BY

PLOS PATHOGENS

RESEARCH ARTICLE

System-wide biochemical analysis reveals ozonide antimalarials initially act by disrupting *Plasmodium falciparum* haemoglobin digestion

Carlo Giannangelo[1☯], Ghizal Siddiqui[1☯], Amanda De Paoli[1], Bethany M. Anderson[2,3], Laura E. Edgington-Mitchell[2,3,4], Susan A. Charman[5], Darren J. Creek[1]*

1 Drug Delivery, Disposition and Dynamics, Monash Institute of Pharmaceutical Sciences, Monash University, Parkville, Victoria, Australia, **2** Drug Discovery Biology, Monash Institute of Pharmaceutical Sciences, Monash University, Parkville, Victoria, Australia, **3** Department of Biochemistry and Molecular Biology, Bio21 Molecular Science and Biotechnology Institute, The University of Melbourne, Parkville, Victoria, Australia, **4** Department of Maxillofacial Surgery, College of Dentistry, New York University, New York, New York, United States of America, **5** Centre for Drug Candidate Optimisation, Monash Institute of Pharmaceutical Sciences, Monash University, Parkville, Victoria, Australia

☯ These authors contributed equally to this work.
* Darren.creek@monash.edu

Check for updates

OPEN ACCESS

Citation: Giannangelo C, Siddiqui G, De Paoli A, Anderson BM, Edgington-Mitchell LE, Charman SA, et al. (2020) System-wide biochemical analysis reveals ozonide antimalarials initially act by disrupting *Plasmodium falciparum* haemoglobin digestion. PLoS Pathog 16(6): e1008485. https://doi.org/10.1371/journal.ppat.1008485

Editor: Timothy J. Egan, University of Cape Town, SOUTH AFRICA

Received: March 17, 2020

Accepted: May 13, 2020

Published: June 26, 2020

Copyright: © 2020 Giannangelo et al. This is an open access article distributed under the terms of the Creative Commons Attribution License, which permits unrestricted use, distribution, and reproduction in any medium, provided the original author and source are credited.

Data Availability Statement: Proteomics and Peptidomics mass spectrometry data and search results have been deposited to the ProteomeXchange Consortium via the PRIDE [104] partner repository with the dataset identifier PXD014313 and project name 'System-wide biochemical analysis reveals ozonide and artemisinin antimalarials initially act by disrupting malaria parasite haemoglobin digestion'. Metabolomics spectrometry data is available at the NIH Common Fund's Metabolomics Data

Abstract

Ozonide antimalarials, OZ277 (arterolane) and OZ439 (artefenomel), are synthetic peroxide-based antimalarials with potent activity against the deadliest malaria parasite, *Plasmodium falciparum*. Here we used a "multi-omics" workflow, in combination with activity-based protein profiling (ABPP), to demonstrate that peroxide antimalarials initially target the haemoglobin (Hb) digestion pathway to kill malaria parasites. Time-dependent metabolomic profiling of ozonide-treated *P. falciparum* infected red blood cells revealed a rapid depletion of short Hb-derived peptides followed by subsequent alterations in lipid and nucleotide metabolism, while untargeted peptidomics showed accumulation of longer Hb-derived peptides. Quantitative proteomics and ABPP assays demonstrated that Hb-digesting proteases were increased in abundance and activity following treatment, respectively. Ozonide-induced depletion of short Hb-derived peptides was less extensive in a drug-treated *K13*-mutant artemisinin resistant parasite line (Cam3.II^{R539T}) than in the drug-treated isogenic sensitive strain (Cam3.II^{rev}), further confirming the association between ozonide activity and Hb catabolism. To demonstrate that compromised Hb catabolism may be a primary mechanism involved in ozonide antimalarial activity, we showed that parasites forced to rely solely on Hb digestion for amino acids became hypersensitive to short ozonide exposures. Quantitative proteomics analysis also revealed parasite proteins involved in translation and the ubiquitin-proteasome system were enriched following drug treatment, suggestive of the parasite engaging a stress response to mitigate ozonide-induced damage. Taken together, these data point to a mechanism of action involving initial impairment of Hb catabolism, and indicate that the parasite regulates protein turnover to manage ozonide-induced damage.

Repository and Coordinating Center website, the Metabolomics Workbench http://metabolomicsworkbench.org, where it has been assigned Project ID PR000809. The data can be accessed directly via its project DOI: 10.21228/M83X38.

Funding: Funding support was provided by the Australian National Health and Medical Research Council (NHMRC) project grants #APP1128003 to DJC, SAC and LE-M, and #APP1160705 and fellowship #APP1148700 to DJC. LE-M is funded by an Australian Research Council (ARC) Discovery Early Career Researcher Award (DECRA) Fellowship (DE180100418) and the Grimwade Fellowship funded by the Russell and Mab Grimwade Miegunyah Fund at the University of Melbourne. The funders had no role in study design, data collection and analysis, decision to publish, or preparation of the manuscript.

Competing interests: The authors have declared that no competing interests exist.

Author summary

The ozonides are a novel class of fully synthetic antimalarial drugs with potent activity against all parasite species that cause malaria, including the deadliest, *Plasmodium falciparum*. With the emergence of resistance to current frontline artemisinin-based antimalarials, new drugs are urgently needed and a clear understanding of their mechanism of action is essential so that they can be optimally deployed in the field. Here, we studied the biochemical effects of two ozonides, OZ277 (marketed in India in combination with piperaquine) and OZ439 (in Phase IIb clinical trials) in *P. falciparum* parasites using an untargeted multi-omics approach consisting of proteomics, peptidomics and time-dependent metabolomics, along with activity-based protease profiling. We found that the ozonides initially disrupt haemoglobin metabolism and that they likely engage the parasite proteostatic stress response. Furthermore, when the duration of ozonide exposure was extended beyond 3 hours to reflect clinically-relevant exposure periods, additional parasite biochemical pathways were perturbed. This comprehensive analysis provides new insight into the antimalarial mode of action of ozonides and provides new opportunities for interventions to enhance their antimalarial efficacy.

Introduction

Promising improvements in malaria control have been recorded over the last two decades, but recent data indicates that the declining mortality rates have either stalled or increased in many malaria endemic regions since 2016 [1]. The absence of a reliable and highly efficacious vaccine means that treatment is heavily reliant on effective antimalarial chemotherapy. Currently, the World Health Organisation (WHO) recommends artemisinin-based combination therapies (ACTs) as the first-line treatment for uncomplicated *Plasmodium falciparum* malaria in all endemic areas [2]. The artemisinins (including dihydroartemisinin, DHA) contain an essential peroxide bond that undergoes reductive activation by haem released through parasite haemoglobin (Hb) digestion [3–6]. This activation process generates highly reactive drug-derived radicals that mediate rapid parasite killing [7]. However, artemisinins are limited by poor biopharmaceutical properties and short *in vivo* half-lives (< 1 h) [7–9]. Furthermore, the emergence of artemisinin resistant parasites now threatens global malaria control and elimination efforts [10]. Thus, there is a desperate need for improved therapeutics to combat malaria.

To overcome some of these limitations, the artemisinin peroxide bond inspired the design of fully synthetic and structurally dissimilar peroxide-based antimalarials, known as ozonides [11] (Fig 1). The first-generation ozonide, OZ277 (later known as RBx11160 or arterolane) [11], was the first to be approved clinically, and although not currently recommended by WHO, is currently marketed as a fixed dose combination with piperaquine (Synriam) in India and parts of Africa. The *in vivo* half-life of OZ277 is only 2- to 3-fold longer than that for DHA [12, 13]. This rapid clearance is thought to be associated with both hepatic metabolism [14] and instability of the peroxide bond when exposed to endogenous sources of iron in blood and tissues [15]. A design strategy aimed at stabilising the peroxide bond to iron-mediated degradation led to the development and selection of the second-generation ozonide, OZ439 (artefenomel) [15]. When tested clinically, OZ439 exhibited an *in vivo* half-life of 46–62 h in humans [16, 17]. OZ439 is currently in Phase IIb clinical trials in combination with ferroquine (ClinicalTrials.gov Identifier: NCT02497612).

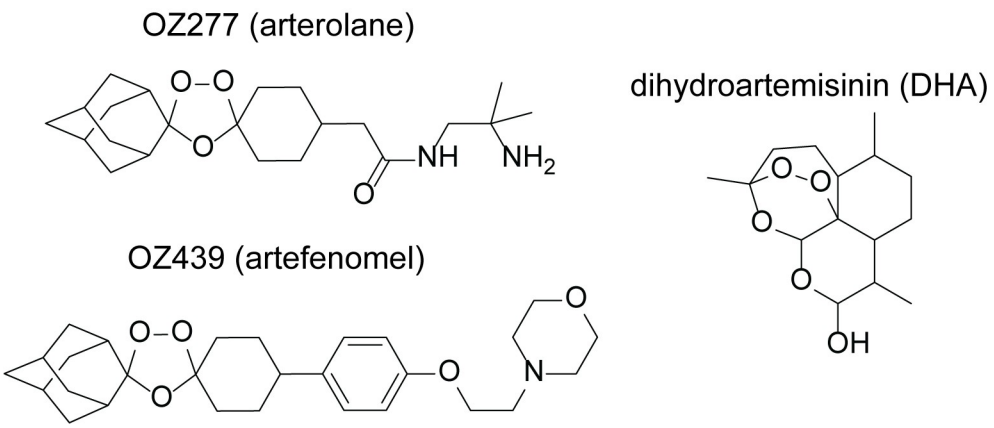


Fig 1. Chemical structures of selected peroxide antimalarials. The fully synthetic ozonide antimalarials, OZ277 (arterolane) and OZ439 (artefenomel), and the clinically used semisynthetic artemisinin derivative, dihydroartemisinin (DHA).

https://doi.org/10.1371/journal.ppat.1008485.g001

Ozonide antimalarials display similar clinical efficacy to DHA, rapidly clearing blood-stage parasites [17, 18]. However, their antimalarial mechanism of action (MoA) has been less extensively studied than the artemisinins, and debate remains about the key molecular events responsible for artemisinin action [19–24]. The current model for ozonide antimalarial activity is that Hb-derived free haem mediates reductive activation of the peroxide bond giving rise to toxic carbon-centred radicals [25] that alkylate a number of essential parasite proteins from various biochemical pathways [26, 27]. Crucially, optimal clinical utilisation of ozonides will rely on a clear understanding of the biochemical mechanisms that underpin their activity. Therefore, we investigated the temporal biochemical response of *P. falciparum* parasites treated with OZ277 and OZ439 using systems-wide analyses, incorporating time-dependent metabolomics and proteomics. We identified Hb digestion as the key initial pathway targeted by ozonide antimalarials and demonstrated that when parasites are forced to rely solely on Hb digestion for nutrients, they become hypersensitive to pulsed ozonide treatment. Furthermore, we showed that ozonides perturb additional pathways when treatment was extended beyond 3 h, reflecting more clinically-relevant exposures for the ozonides, and that parasites likely regulate protein turnover to manage ozonide-mediated damage. This work provides new opportunities for interventions to target malaria parasites and enhance ozonide antimalarial efficacy.

Results

Ozonide antimalarials initially deplete short haemoglobin (Hb)-derived peptides

In order to distinguish the early peroxide-induced effects from secondary mechanisms, we employed a time-dependent, untargeted metabolomics approach that allowed comprehensive biochemical profiling of the primary pathways affected by ozonide antimalarials in *P. falciparum* infected red blood cells (iRBCs) (S1 Fig). Trophozoite-stage parasites (28–34 h post invasion) were treated with 300 nM of OZ277 or OZ439 or 100 nM of DHA over a time course of up to 3 h (n = at least four biological replicates). These drug concentrations are equivalent to the IC_{50} for a 3 h pulse, under the same *in vitro* conditions used in the metabolomics analysis (10% parasitaemia and 2% Hct) [28], and are within therapeutic concentration ranges [10, 17, 29]. Univariate analysis of the untargeted metabolomics dataset (S1 Dataset) revealed a temporal increase in the percentage of drug-induced metabolic changes (S2A Fig) and that

widespread metabolic perturbations were not evident after short drug exposures (S2B Fig). The ozonides rapidly and disproportionately affected peptide metabolism, with approximately 15–25% of all putatively identified short peptides (2–4 amino acids in length) significantly perturbed within 3 h of drug treatment (P-value < 0.05) (S2B Fig). These significantly perturbed peptides were parasite-specific metabolites (S1 Dataset) and exhibited a progressive depletion in abundance over the 3 h drug exposure (Fig 2A and 2B). Interestingly, the extent of peptide depletion was more extensive and faster in DHA-treated parasites compared to the ozonides, which is consistent with the more rapid kinetics of antiparasitic activity previously observed for DHA compared to the ozonides for these short pulse exposures (< 3 h) [30]. The amino acid sequence of a subset of these putatively identified peptides was confirmed by MS/MS and the majority of perturbed peptides (i.e., those that were decreased by at least 1.5-fold) could be mapped to either the alpha or beta chains of Hb (Fig 3A).

A similar, although less extensive, temporal increase in the number of significant metabolic perturbations was confirmed in ring-stage parasites (6–12 h post invasion) treated with ozonide antimalarials (S3A Fig), with putative Hb-derived peptides representing the first metabolites to be significantly perturbed (S1 Dataset and S3B Fig). This was further verified using multivariate analysis, where sparse partial least squares–discriminant analysis (sPLS-DA) revealed that Hb-derived short peptides were responsible for the greatest differences between the ozonide-treated samples and controls (S4 Fig). Similar to trophozoite-stage parasites, these Hb peptides showed a time-dependent depletion in the treated parasite cultures compared to controls (Fig 3C).

To further investigate the importance of parasite Hb digestion to ozonide antimalarial action, untargeted metabolomic profiling was also performed on artemisinin resistant (Cam3.II^{R539T}) and isogenic sensitive (Cam3.II^{rev}) [31] early trophozoite-stage (22–26 h post invasion) parasites (S2 Dataset). Artemisinin resistant early trophozoite-stage parasites have been shown to exhibit differential sensitivity to short DHA exposures compared to the isogenic sensitive strain, albeit a less dramatic difference than early rings [32]. Targeted analysis of the LC-MS raw data identified 26 perturbed peptides (at least 1.5-fold) in drug-treated resistant (Cam3.II^{R539T}) or sensitive parasites compared to control (Fig 2D). The majority ($> 70\%$) of perturbed peptides were depleted in treated samples compared to the control (Fig 2D and S5A Fig) and most of these peptides (all except two) could be mapped to Hb (S5B Fig). Notably, the extent of peptide depletion was greater in the sensitive parasites than in the resistant line (Fig 2D). In general, the abundance of these peptides in treated resistant parasites remained at, or above, the basal levels detected in untreated sensitive parasites.

Ozonide antimalarial treatment causes accumulation of long chain Hb peptides

The rapid depletion of short chain Hb-derived peptides led us to consider how ozonide antimalarial exposure impacts longer Hb-derived peptides. We used a MS/MS-based global peptidomics approach (S1 Fig) to examine the abundance of endogenous peptides (< 10 kDa) within ozonide-treated *P. falciparum* parasites. Peptidomics analysis identified a total of 59 endogenous *P. falciparum* peptides and 59 endogenous human peptides (S3 Dataset). OZ277 (300 nM for 3 h) treatment significantly altered the abundance of 30 endogenous peptides in trophozoites-stage parasites (P-value < 0.05), 17 of which originated from Hb (alpha and beta), and were increased in abundance (Fig 3B). A similar build-up of long chain Hb peptides was also observed following treatment with OZ439 (300 nM for 3 h). Unlike the ozonides, exposure of trophozoite-stage parasites to 3 h of DHA (100 nM) predominantly depleted the abundance of Hb-derived peptides, with 26 peptides significantly depleted and four

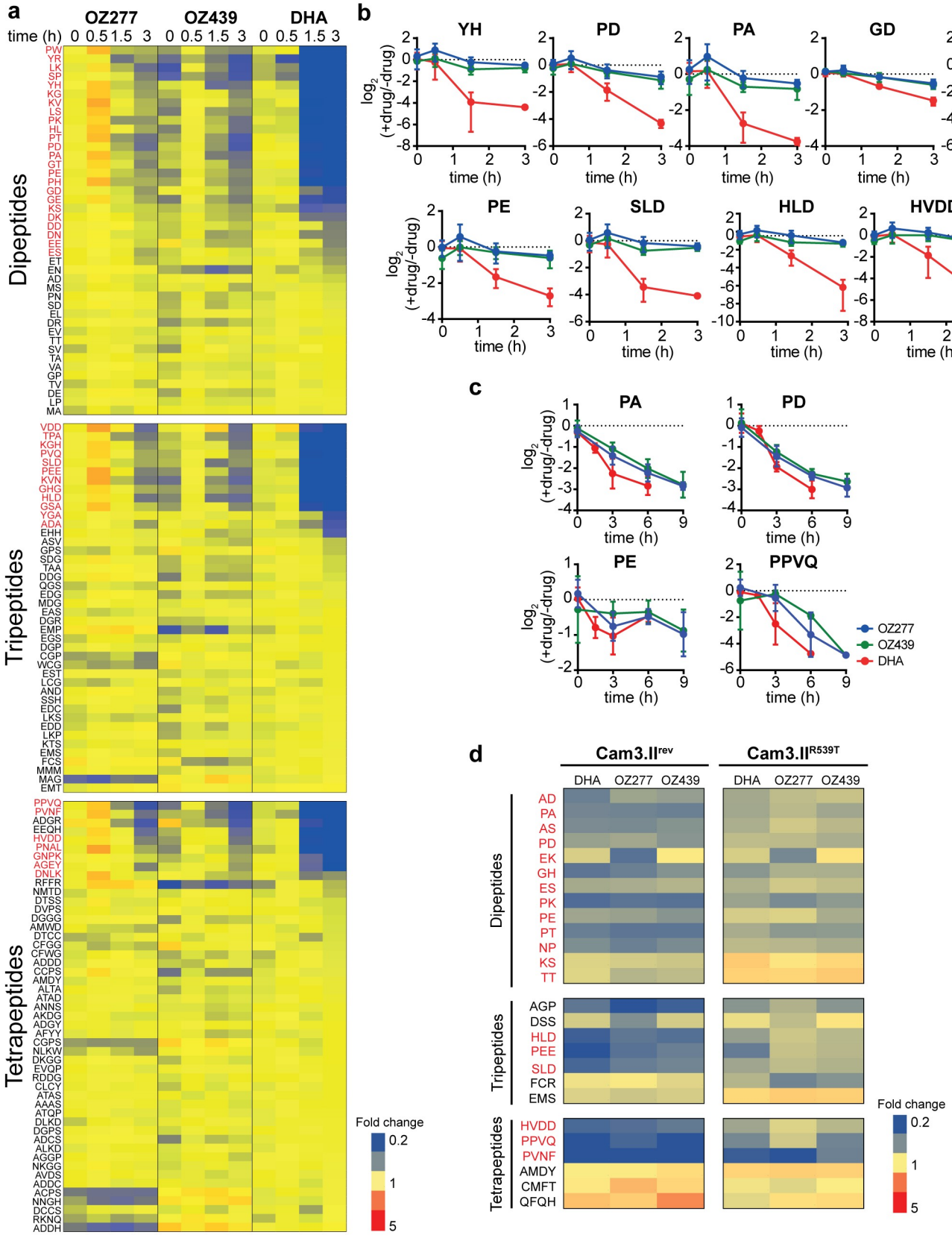

a
OZ277
OZ439
DHA
time (h) 0 0.5 1.5 3 0 0.5 1.5 3 0 0.5 1.5 3
Dipeptides
Tripeptides
Tetrapeptides
Fold change
0.2
1
5
b
YH
PD
PA
GD
TPA
PE
SLD
HLD
HVDD
log2 (+drug/-drug)
time (h)
OZ277
OZ439
DHA
c
PA
PD
PE
PPVQ
log2 (+drug/-drug)
time (h)
OZ277
OZ439
DHA
d
Cam3.II^rev
Cam3.II^R539T
DHA OZ277 OZ439
DHA OZ277 OZ439
Dipeptides
AD PA AS PD EK GH ES PK PE PT NP KS TT
Tripeptides
AGP DSS HLD PEE SLD FCR EMS
Tetrapeptides
HVDD PPVQ PVNF AMDY CMFT QFQH
Fold change
0.2
1
5

Fig 2. Peroxide-induced perturbations to peptide metabolism. a, Heatmap showing the average fold change for all identified peptides at each time point after treatment of trophozoite-infected cultures (*P. falciparum* 3D7 strain) with OZ277, OZ439 and DHA. Values represent the average of at least three biological replicates, expressed relative to the average untreated control value (at least seven biological replicates) for that respective time point. Putative haemoglobin peptides are shown in red text. **b**, Representative time profiles showing the progressive depletion in abundance of selected putative haemoglobin-derived peptides after peroxide treatment of trophozoite-stage parasites (3D7). Values are the average fold change (± SD) relative to the untreated control of at least three biological replicates. **c**, Time-dependent decrease in the abundance of the four haemoglobin-derived peptides consistently depleted following peroxide treatment in ring infected cultures (3D7). Values are the average fold change (± SD) relative to the untreated control of four biological replicates. **d**, Heatmap of the peptides that were altered in abundance (≥ 1.5-fold relative to the untreated control) following peroxide treatment in the *K13*-wildtype artemisinin sensitive (Cam3.II^{rev}) and *K13*-mutant artemisinin resistant (Cam3.II^{R539T}) parasite lines. Data shown are the average for three or five biological replicates expressed relative to the average for the untreated control from the same parasite line. Putative haemoglobin peptides are shown in red text.

https://doi.org/10.1371/journal.ppat.1008485.g002

significantly elevated relative to control (Fig 3B). The differential impact of ozonides and DHA on longer chain Hb-derived peptides may be explained by the faster onset of action of artemisinins compared to ozonides [30]. Indeed, a shorter DHA exposure (1 h) caused an accumulation of longer Hb peptides similar to the ozonides (Fig 3C and S4 Dataset).

We also assessed whether the accumulated Hb components in peroxide-treated parasites differ from those in E64d (cysteine protease inhibitor)-treated parasites. E64d causes parasite digestive vacuoles to accumulate undegraded Hb and swell due to disruption of the initial endoproteolytic cleavage of Hb [33, 34]. Trophozoite-stage parasites treated with E64d for up to 3 h developed a characteristic swollen digestive vacuole (S6A Fig), consistent with abrogated digestion of full-length Hb. These same parasites exhibited a modest trend towards accumulation of intact Hb and minor changes in free haem and haemozoin levels (S6A Fig) when these haem-containing species were measured using haem fractionation assays [35]. Visualisation of monomer Hb (17 kDa) by Coomassie staining of SDS-PAGE gels confirmed that undigested Hb accumulated in trophozoites after these short E64d exposures (S6B Fig). Conversely, peroxide-treated parasites showed a minor decrease in the levels of full-length Hb, when measured using the haem fractionation assay (no changes in other haem species were evident) (S6A Fig), which is broadly consistent with our quantitative proteomics data (S6C Fig). Peroxide exposures of up to 3 h caused no changes in digestive vacuole morphology, indicating that there is no inhibition of proteolysis of full-length Hb (S6A Fig). Taken together, these findings suggest that the accumulated Hb components in peroxide-treated parasites are likely different from those resulting from specific inhibition of cysteine proteases.

Our untargeted peptidomics analysis also showed that ozonide treatment perturbed the levels of some endogenous parasite peptides. Of the 13 parasite peptides significantly perturbed following OZ277 exposure, five originated from an uncharacterised *P. falciparum* protein (PF3D7_0716300) and were decreased in abundance compared to control (S3 Dataset). OZ439 treatment resulted in significant perturbations to five parasite peptides, four of which were from this same uncharacterised protein (PF3D7_0716300) and were decreased relative to the untreated (S3 Dataset). A total of 15 endogenous parasite peptides were altered in abundance following DHA treatment, including six peptides that originated from the uncharacterised protein PF3D7_0716300 and, similar to ozonide exposure, were significantly decreased compared to control (S3 Dataset).

Ozonide antimalarial treatment increases the abundance and activity of Hb proteases

Plasmodium parasites digest Hb through a semi-ordered proteolytic process incorporating numerous proteases of different classes [36]. Peptidomics and metabolomics analyses of treated parasites suggested that ozonide antimalarials disrupt Hb catabolism through inhibition of the proteases involved in the breakdown of large to small Hb peptides. In order to quantify the abundance of the proteases involved in Hb digestion, we used dimethyl labelling-

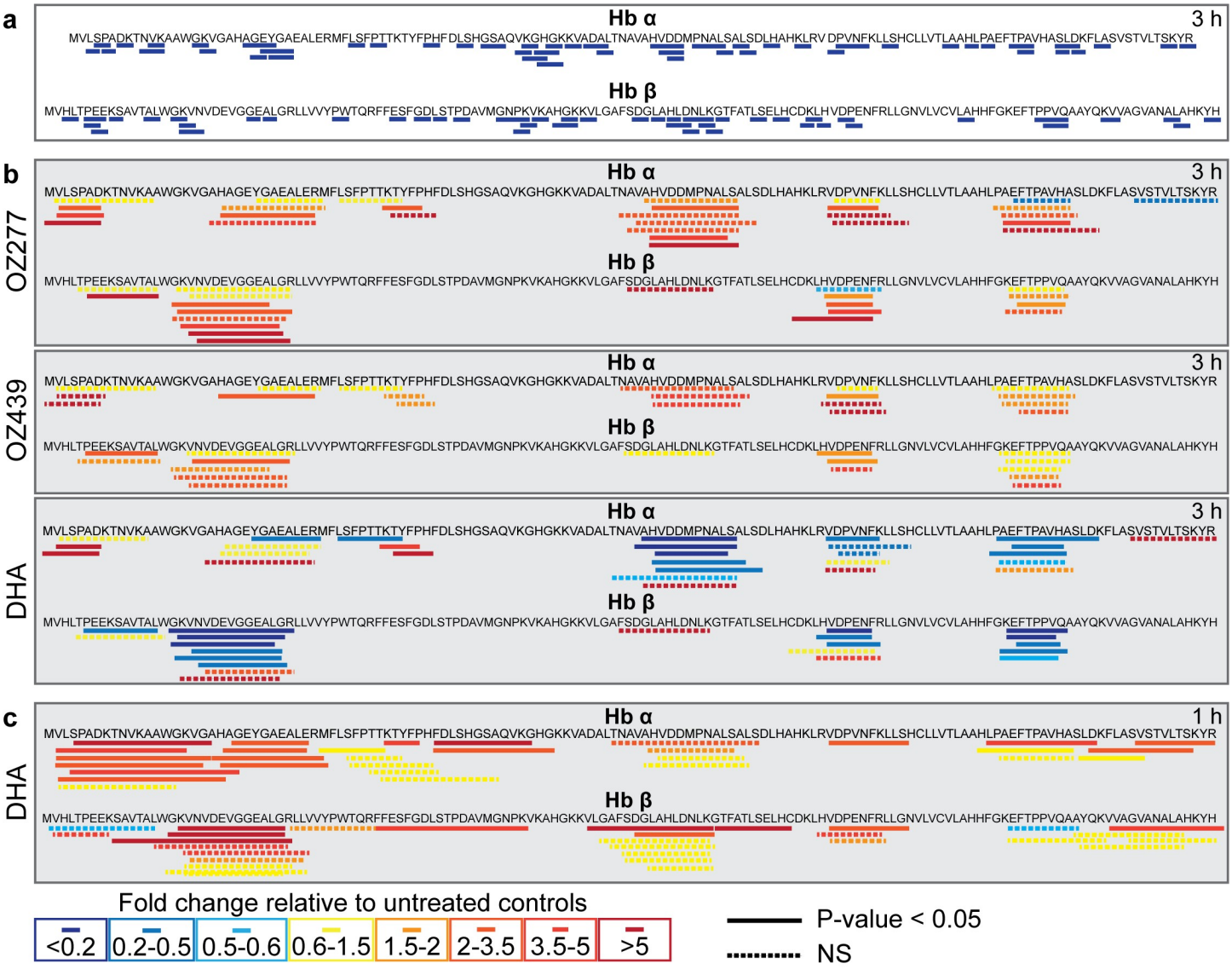


Fig 3. Sequence coverage and relative abundance of haemoglobin alpha (Hb α) and haemoglobin beta (Hb β) peptides detected after peroxide treatment. a, Sequence coverage for putative haemoglobin-derived di-, tri-, and tetra-peptides that were differentially abundant (≥ 1.5-fold) following peroxide antimalarial treatment relative to the untreated control (3D7 parasites). The peptide sequences PA, PT, PE, PEE, HLD, SLD, PPVQ, PVNF and HVDD have been confirmed by MS/MS analysis. For all other putative peptide sequences, all potential isomers have been mapped. **b**, Sequence coverage for all long Hb α and Hb β peptides detected in peptidomics studies. Peptide abundances are the average fold change following 3 hours of drug treatment (OZ277, OZ439 and DHA), expressed relative to the untreated control (DMSO) from at least three biological replicates (3D7 parasites). **c**, Sequence coverage for Hb α and Hb β peptides detected following 1 hour of DHA treatment in Cam3.II^{rev} (artemisinin sensitive) parasites. Peptide abundances are the average fold change expressed relative to the untreated control (DMSO) from two biological replicates. In **b**, **c**, samples were normalised according to peptide concentration (measured using a bicinchoninic acid assay) during sample preparation. The solid lines represent the amino acid sequences of peptides that significantly changed in abundance after drug treatment relative to the untreated control (P-value < 0.05). Dashed lines represent non-significant (NS) changes. Increased and decreased peptide abundance are represented by red and blue (solid or dashed) lines, respectively.

https://doi.org/10.1371/journal.ppat.1008485.g003

based quantitative proteomics (S1 Fig) [37]. Targeted analysis of the global proteomics data (S7 Fig and S5 Dataset) identified falcipains 2 and 3 (FP 2 and FP 3) and the plasmepsins (PM I, PM II, PM IV and HAP), proteases thought to be involved in the initial stages of Hb degradation [36], to be elevated in abundance in drug-treated samples compared to control (Fig 4A). Dipeptidyl aminopeptidase 1 (DPAP1), which removes dipeptides from the polypeptides produced by upstream proteases [38], and the alanyl aminopeptidase (*Pf*A-M1), leucyl

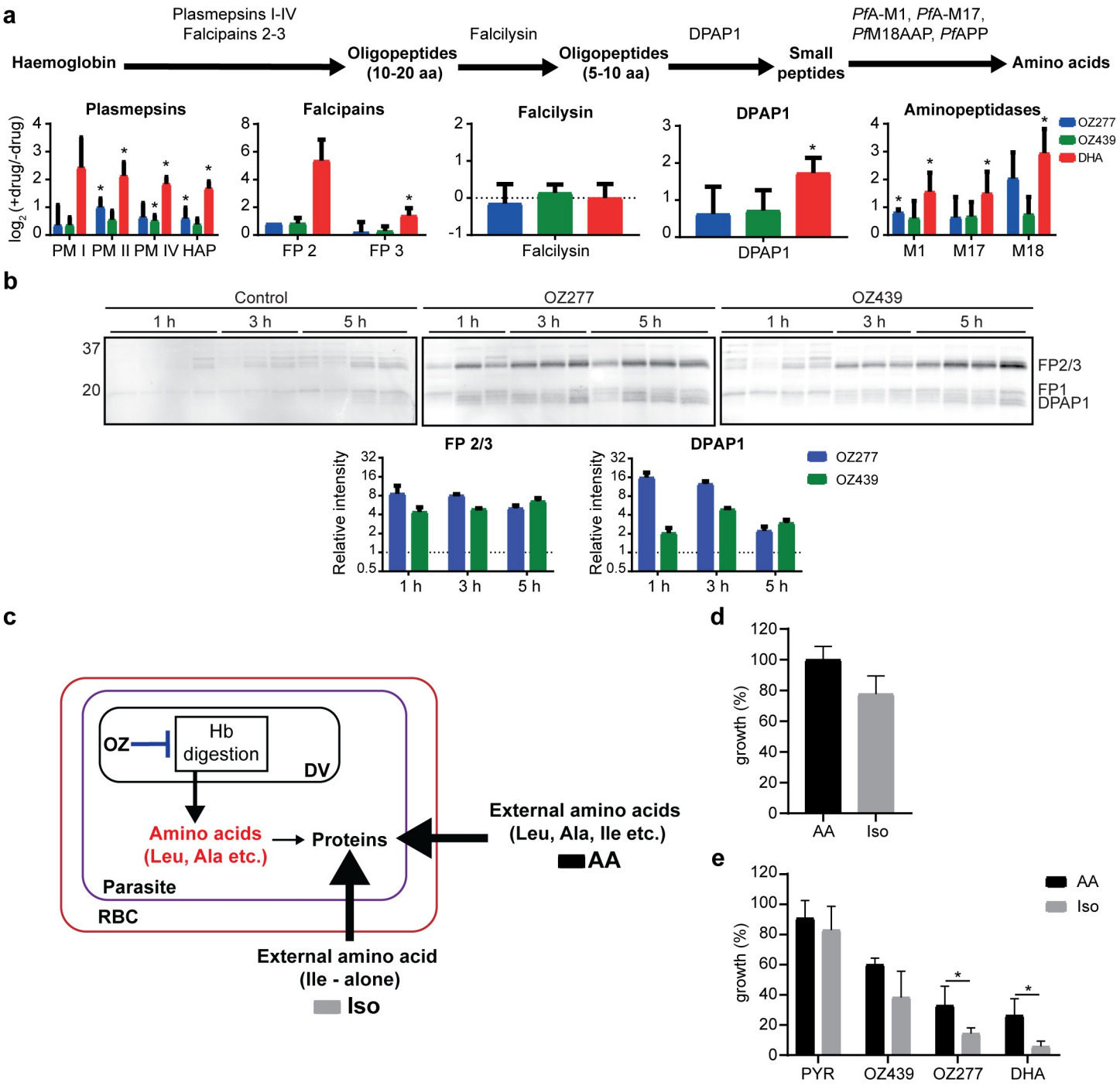


Fig 4. Peroxide antimalarials act by perturbing haemoglobin digestion. a, Disruption of protease abundance in the haemoglobin digestion pathway [36]. Values are the average $\log_2$ fold change (± SD) relative to the untreated control of at least three biological replicates. Trophozoite infected cultures (*P. falciparum* 3D7) were incubated with OZ277, OZ439 (both 300 nM) or DHA (100 nM) for 3 h. Falcipain 2 (FP 2) was identified in only two OZ277 treatment experiments, therefore the mean alone is shown. Aminopeptidase P (*Pf*APP) was not identified in any of the proteomic experiments. DPAP1, dipeptidyl aminopeptidase 1; FP, falcipain; HAP, histo-aspartic protease; *Pf*APP, aminopeptidase P; *Pf*A-M1, alanyl aminopeptidase; *Pf*A-M17, leucyl aminopeptidase; *Pf*M18APP, aspartyl aminopeptidase; PM, plasmepsin; * P-value < 0.05. **b**, Parasite cysteine protease activity after peroxide treatment using the activity-based probe (ABP), DCG04. Cysteine protease activity and densitometric analysis of the falcipain (FP) 2/3 and dipeptidyl aminopeptidase 1 (DPAP1) signal after OZ277 and OZ439 treatment in *P. falciparum* trophozoite stage parasites (3D7) using DCG04 in lysates at pH 5.5 (acidic). Trophozoite infected cultures were incubated with OZ277, OZ439 (both 300 nM) or an equivalent volume of DMSO (control). DCG04 labelling was detected by blotting membranes with streptavidin-AF647 after SDS-PAGE and transfer. The lanes for each time point are independent drug treatments and represent at least three biological replicates per time point that were run on the same gel side-by-side. For the densitometric analysis, the post drug

treatment FP 2/3 and DPAP1 signal intensity was normalised to the average signal intensity of the appropriate time point in the untreated control (±SD). **c**, Schematic showing that infected RBCs treated with DHA or ozonides (OZ) can use exogenous amino acids when cultured in AA medium (Full RPMI medium with all 20 amino acids) in response to disrupted haemoglobin digestion (arrow shown in blue), while parasites in Iso medium (supplemented with isoleucine alone at a final concentration of 147.5 μM) must rely solely on haemoglobin digestion for amino acids. **d**, Amino acid requirement for cultured *P. falciparum* 3D7 parasites. Parasite viability measured following 48 h incubation in medium containing all amino acids (AA, black bars) and isoleucine alone medium (Iso, grey bars). **e**, Parasite sensitivity to peroxides when cultured in AA (black bars) medium compared to Iso (grey bars) medium. Trophozoite infected cultures (3D7) were incubated with pyrimethamine (PYR), OZ277, OZ439 (all 300 nM), DHA (100 nM) or an equivalent volume of DMSO (control) for 3 h. Data represents the mean ± SD of at least three biological replicates. Growth values for each treatment is expressed relative to the appropriate untreated medium (Iso or AA) control, which was set to 100%. * P-value < 0.05.

https://doi.org/10.1371/journal.ppat.1008485.g004

aminopeptidase (*Pf*A-M17) and aspartyl aminopeptidase (*Pf*M18AAP) metalloproteases, all of which are involved in the terminal stages of Hb digestion [39], were all increased following ozonide treatment (Fig 4A). No changes in the abundance of falcilysin (Fig 4A) was detected (S5 Dataset).

As most Hb-degrading proteases were elevated in abundance after ozonide antimalarial treatment, we then investigated the temporal impact of ozonides on Hb protease activity using activity-based probes (ABPs) targeting parasite cysteine proteases [40] (S1 Fig). Trophozoite-stage parasite cultures were treated with OZ277 or OZ439 (300 nM) for up to 5 h and the biotinylated epoxide ABP, DCG04 [41], was used to label the Hb-digesting cysteine proteases FP 2, FP 3 and DPAP1 in the parasite lysate under both acidic (pH 5.5) and neutral pH (pH 7.2) conditions. Both OZ277 and OZ439 caused a time-dependent increase in the activity of proteases with molecular weights consistent with that of the FPs (FP 2 and FP 3), and DPAP1 [42] (Fig 4B). A similar increase in the activity of these proteases was observed under acidic (the pH environment of the parasite digestive vacuole) or neutral pH conditions (S8A Fig), and activity was inhibited by pre-treatment of the parasite lysate with the cysteine protease inhibitor, ALLN (S8B Fig). FPs and DPAP1 activity were increased within 1 h of OZ277 treatment compared with DMSO controls (Fig 4B). In contrast, OZ439 increased FPs and DPAP1 activity after 3–5 h of drug exposure, consistent with it having a slower onset of action within the parasite [30]. Ozonide-induced increases in activity of FPs and DPAP1 were further confirmed by another cysteine protease-targeting probe, FY01 [42], under both acidic (S9A Fig) and neutral (S9B Fig) conditions. While total protein levels between the treatment and control groups were normalised prior to incubation with the ABP, it is likely that increased FP and DPAP abundance in response to peroxide treatment (as determined by quantitative proteomics; Fig 4A) is a major contributing factor to the increase in protease activity observed in these experiments.

Impaired Hb digestion underpins initial ozonide-induced toxicity

Functional Hb uptake and digestion is essential for parasite survival as it supplies amino acids for protein synthesis [43]. As our multi-omics and ABPP analyses identified Hb catabolism as the primary pathway affected by ozonide antimalarial treatment, we hypothesised that drug-derived radicals initially target this pathway, disrupting Hb catabolism, and starving the parasite of Hb-derived amino acids. To test this, we determined the potency of peroxide antimalarials on parasites grown in full RPMI medium (with all 20 amino acids) (AA medium) and parasites cultured in medium lacking all exogenous amino acids except for isoleucine (the only amino acid absent from Hb) (Iso medium), thereby forcing parasites to rely solely on Hb catabolism for amino acid supply (Fig 4C).

Similar to published results [43], parasites cultured in Iso medium had a minor growth defect of approximately 20% compared to parasites cultured in AA medium (Fig 4D). Trophozoite-stage cultures exposed to OZ277 or OZ439 (both 300 nM) for 3 h were sensitised by 2.3- and 1.6-fold, respectively, in the Iso medium (Fig 4E), suggesting that compromised Hb

catabolism is the primary MoA of ozonides in the initial exposure phase. However, when drug pressure was maintained throughout the entire RBC life cycle, there was no difference in sensitivity between parasites cultured in the Iso and AA mediums (S10 Fig), suggesting that mechanisms beyond disrupted Hb digestion contribute to parasiticidal activity during prolonged exposure. DHA treated parasites were almost 5-fold more sensitive in the Iso medium compared to parasites cultured in AA medium (Fig 4E). In contrast, the potency of pyrimethamine, which kills parasites by a mechanism independent of Hb digestion [44], was not affected when cultured in either AA or Iso medium (Fig 4E).

Ozonide antimalarial treatment upregulates parasite proteasome and translation machinery proteins

Untargeted analysis of our global quantitative proteomics dataset (S5 Dataset) identified a total of 1293, 1284 and 1613 proteins (including human and *P. falciparum* proteins) with at least two unique peptides in a minimum of three independent biological experiments in OZ277, OZ439 (both 300 nM) and DHA (100 nM) treated parasites, respectively. Peroxide treatment caused significant dysregulation (P-value $\leq$ 0.05 and fold-change $\geq$ 1.5) to a subset of proteins within 3 h of drug exposure (S7 Fig). Perturbation of the parasite proteome was most dramatic after DHA treatment, with 12% of the 1552 *P. falciparum* proteins detected being significantly increased in abundance and 6% significantly downregulated compared to the untreated level. Of the 1255 *P. falciparum* proteins detected after OZ277 treatment, 7% were increased in abundance and 1.6% were decreased compared to the control. OZ439 had the least pronounced impact on the parasite proteome (1243 *P. falciparum* proteins detected), with 1.6% and $<$ 1% of proteins significantly increased and decreased relative to control levels, respectively.

Clustering analysis of all proteins significantly perturbed (P-value $\leq$ 0.05 and fold-change $\geq$ 1.5) by OZ277 treatment revealed that translation regulation (P-value = $5.184E^{-7}$) and the proteasome system (P-value = $5.288E^{-4}$) were the two main pathways affected. Parasite proteins in these two networks were significantly enriched following OZ277 treatment (Fig 5). Similar protein clustering was also observed for DHA (S11 Fig) treatment, with elevated levels of proteins involved in translation regulation (P-value $< 1.0E^{-9}$) and the proteasome system (P-value $3.691E^{-6}$). A trend towards increased abundance of translation regulation and proteasome system proteins was also observed following 3 h of OZ439 exposure (S5 Dataset), however no protein networks were significantly enriched.

Extended exposure disrupts secondary metabolic pathways involved in ozonide antimalarial activity

Using untargeted metabolomic profiling, we also investigated whether parasite biochemical pathways other than Hb metabolism were affected following long-term ozonide treatment ($>$ 3 h). Extended exposure induced metabolic perturbations beyond peptide metabolism, including, amino acid, lipid, cofactor and vitamin, and nucleotide metabolism (Fig 6A and S1 Dataset). It is possible that some of these secondary responses to prolonged drug treatment represent nonspecific responses from dying parasites, but it is noted that different drug-specific responses were reported in similar metabolomics studies of other compounds [45–47], suggesting that these metabolic alterations are largely ozonide-specific. Extended treatment of trophozoite-stage parasites with OZ277 and OZ439 resulted in significant perturbations (P-value $\leq$ 0.05 and fold-change $\geq$ 1.5) to approximately 5% of the 217 putatively identified lipids (S12 Fig). The major parasite neutral glycerolipid species, diglycerides (DG) and triglycerides (TG), were depleted within 6 h of ozonide exposure (S12 Fig). DGs are the direct metabolic

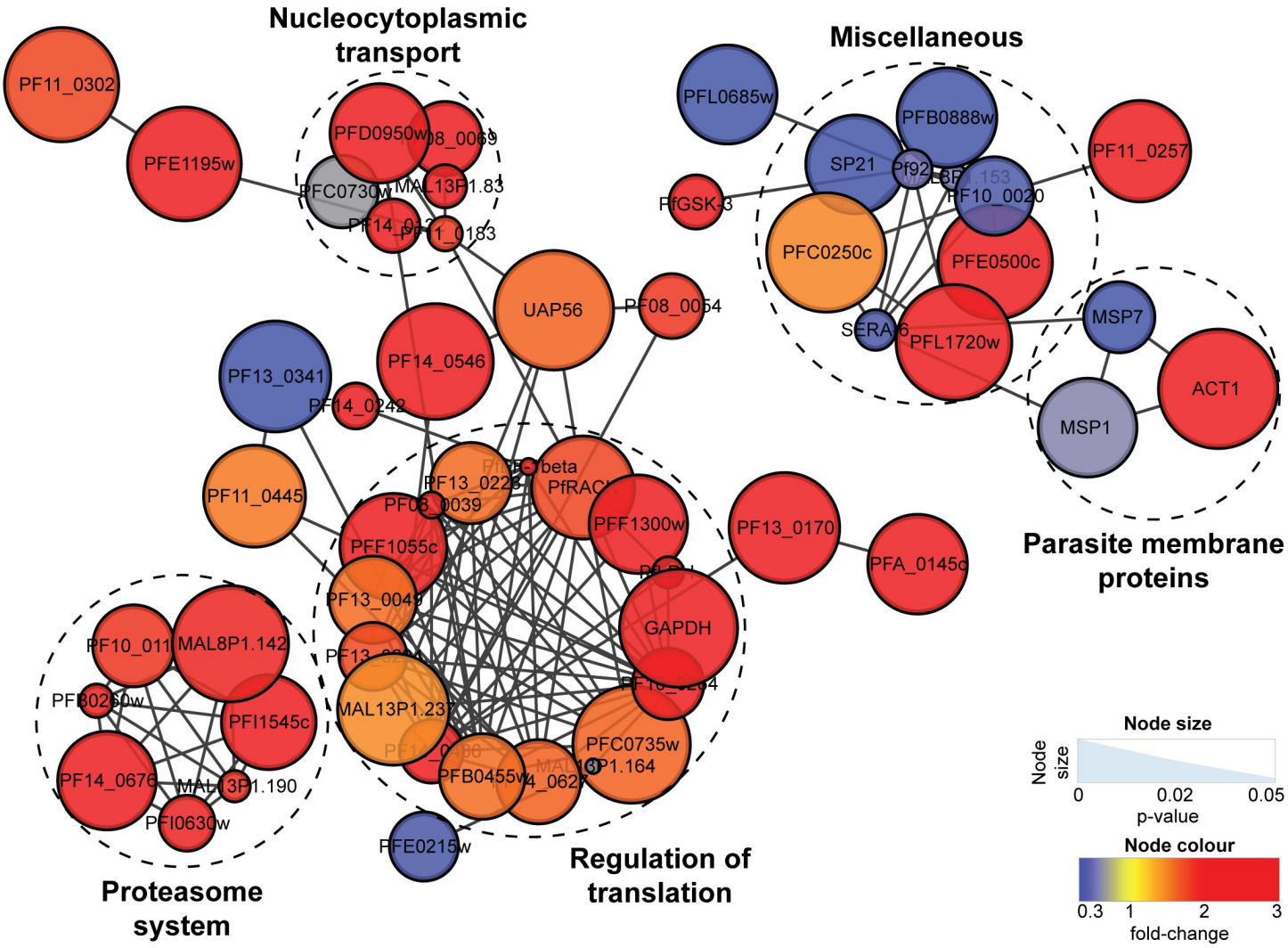


Fig 5. OZ277-induced disruption to the *P. falciparum* (3D7 strain) proteome. Network analysis of trophozoite stage parasite proteins perturbed following treatment with OZ277 (300 nM for 3 h). The network analysis was built using the STRINGdb interaction network analysis output (connectivity was based on experimental, database and co-expression evidence with a minimum interaction score of 0.7) in Cytoscape 3.6 with the ClusterONE algorithm. Node size represents P-value and node colour represents fold-change from at least three independent replicates.

https://doi.org/10.1371/journal.ppat.1008485.g005

precursor of phosphatidylcholine (PC) and phosphatidylethanolamine (PE) lipids, the main glycerophospholipids in the parasite. Metabolites involved in PC and PE *de novo* synthesis accumulated in a time-dependent manner following extended ozonide treatment, while some of the PCs and PEs themselves, and other glycerophospholipids, were depleted (Fig 6B and S12 Fig). At the proteome level, four of the six enzymes in the *de novo* glycerophospholipid synthesis pathway (Kennedy pathway) were elevated after ozonide treatment compared to control (Fig 6B and S13 Fig). Prolonged treatment of rings (> 3 h) also disrupted *de novo* synthesis of PC and PE lipids (S14 Fig).

Extended ozonide exposure also disrupted parasite pyrimidine nucleotide biosynthesis. Metabolites of the *de novo* pyrimidine biosynthesis pathway, L-aspartate, N-carbamoyl-L-aspartate and uridine monophosphate (UMP), were all depleted after drug treatment (Fig 6C and S15 Fig), while at the proteome level, four of the six enzymes in this pathway were elevated compared to the control (Fig 6C and S16 Fig).

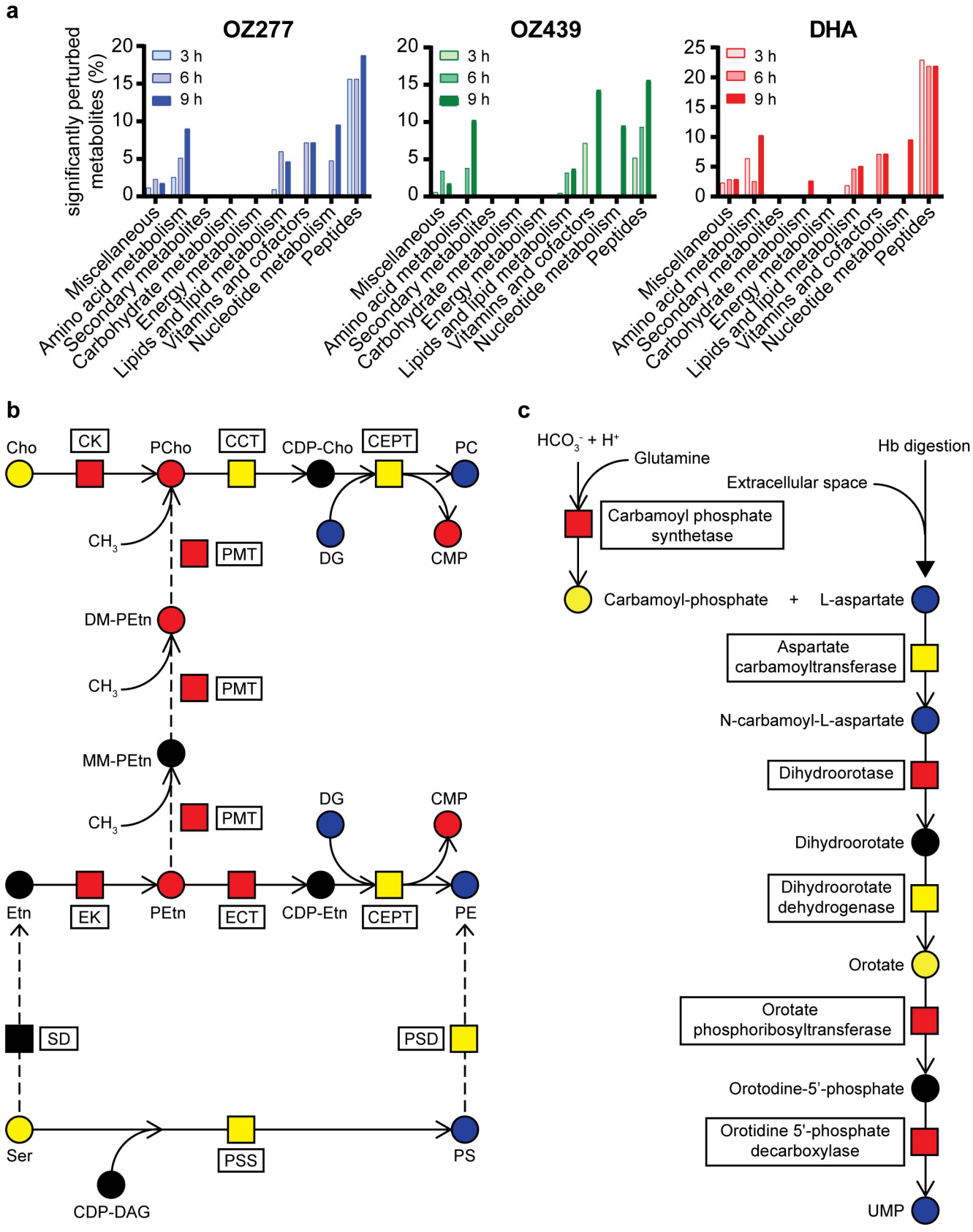

a
OZ277
OZ439
DHA
significantly perturbed metabolites (%)
3 h
6 h
9 h
Miscellaneous
Amino acid metabolism
Secondary metabolites
Carbohydrate metabolism
Energy metabolism
Lipids and lipid metabolism
Vitamins and cofactors
Nucleotide metabolism
Peptides
b
Cho
CK
PCho
CCT
CDP-Cho
CEPT
PC
CH3
PMT
DG
CMP
DM-PEtn
MM-PEtn
Etn
EK
PEtn
ECT
CDP-Etn
PE
SD
PSD
Ser
PSS
PS
CDP-DAG
c
HCO3- + H+
Glutamine
Hb digestion
Extracellular space
Carbamoyl phosphate synthetase
Carbamoyl-phosphate
+
L-aspartate
Aspartate carbamoyltransferase
N-carbamoyl-L-aspartate
Dihydroorotase
Dihydroorotate
Dihydroorotate dehydrogenase
Orotate
Orotate phosphoribosyltransferase
Orotodine-5'-phosphate
Orotidine 5'-phosphate decarboxylase
UMP

Fig 6. Peroxide-induced disruption of secondary biochemical pathways. a, Metabolic perturbations in trophozoite-stage parasite cultures (*P. falciparum* 3D7 strain). Pathway enrichment analysis showing the percentage of significantly perturbed metabolites (Welch's *t* test; P-value < 0.05 and fold change > 1.5) as a function of metabolite class for extended (3, 6 and 9 h) exposure with OZ277, OZ439 (both 300 nM) and DHA (100 nM). **b**, Peroxide-induced disruption of the phosphatidylcholine (PC) and phosphatidylethanolamine (PE) lipid biosynthesis pathways within *P. falciparum* parasites (3D7). The dashed arrows represent an alternative route for the synthesis of PC from ethanolamine (Etn) in *P. falciparum*. CCT, choline-phosphate cytidyltransferase; CDP-, cytidine-diphospho-; CEPT, choline/ethanolamine phosphotransferase; Cho, choline; CK, choline kinase; CMP, cytidine monophosphate; DAG/DG, diglyceride; DM-, dimethyl-; ECT, ethanolamine-phosphate cytidyltransferase; EK, ethanolamine kinase; Etn, ethanolamine; MM-, monomethyl; PC, phosphatidylcholine; PCho, choline phosphate; PE, phosphatidylethanolamine; PEtn, ethanolamine phosphate; PG, phosphatidylglycerol; PMT, phosphoethanolamine N-methyltransferase; PS, phosphatidylserine; PSD, phosphatidylserine decarboxylase; PSS, phosphatidylserine synthase; SD, serine decarboxylase. **c**, Peroxide-induced perturbation of pyrimidine biosynthesis in trophozoite-stage parasite cultures (3D7). Hb, haemoglobin; UMP, uridine monophosphate. In **b**, **c**, metabolites (circles) and proteins (squares) in red and blue were increased and decreased in abundance after drug treatment, respectively. Yellow and black represent no change and not detected, respectively.

https://doi.org/10.1371/journal.ppat.1008485.g006

Discussion

This study provides a detailed assessment of the *P. falciparum* biochemical pathways that are altered in response to ozonide antimalarial treatment. The "multi-omics" analysis revealed that ozonides act by rapidly perturbing parasite Hb catabolism prior to affecting other biochemical pathways, and suggested that the parasite regulates protein turnover to mitigate widespread ozonide-induced damage.

The time-resolved untargeted metabolomics approach allowed the mapping of primary and secondary ozonide-induced effects on parasite metabolism and revealed that short drug exposures induced rapid depletion of short-chain Hb-derived peptides, which was most pronounced in the more susceptible trophozoite-stage, in comparison to the less susceptible [28, 30] ring-stage parasites (Fig 2 and S3 Fig). It is noted that previous metabolomic profiling of ozonide-treated, magnetically purified *P. falciparum* cultures revealed no major alterations to parasite metabolism [47]. However, that was likely due to the high parasitaemia conditions ($> 90\%$) of magnetically purified cultures inducing rapid ozonide degradation such that no measurable antimalarial activity could occur [28]. Consistent with previous reports [45, 46], our metabolomics analysis also showed that DHA induced depletion of short Hb-derived peptides. Interestingly, this occurred more rapidly for DHA than the ozonides (within 1.5 h of exposure versus 3 h of exposure), which agrees with the reported exposure time-dependence of activity for DHA and ozonides [30].

Digestion of host Hb is essential for parasite survival as it provides amino acids for parasite protein synthesis and has additional non-anabolic functions, such as maintaining osmotic stability of the iRBC [48–50]. Hb digestion is most active during the trophozoite-stage [51], resulting in extensive turnover of diverse Hb-derived peptides and the release of a high concentration of haem, which activates peroxide antimalarials within the parasite [3, 30, 52]. The extensive drug activation and Hb turnover in trophozoites likely explains the profound impact of peroxide antimalarials on Hb-derived small peptides in trophozoites (in terms of both the range of Hb peptides affected and magnitude of peptide depletion) compared to the ring-stage (Fig 2). Although it is generally assumed that little Hb digestion occurs within ring-stage parasites, expression of active Hb-degrading proteases [30] and small haemozoin crystals (by-products of Hb digestion) have been detected [53–55]. This indicates that a low level of active Hb degradation occurs in ring-stage parasites and supports the observation of depleted Hb-derived small peptides following ozonide treatment (Fig 2C and S3 and S4 Figs).

The accumulation of longer Hb-derived peptides (Fig 3B) and depletion of shorter di, tri and tetrapeptides (Fig 2) suggests that the ozonides disrupt Hb catabolism through an inhibitory effect on the proteases involved in the conversion of large to small Hb peptides. However, we cannot rule out inhibition of the peptide transporters on the digestive vacuole membrane, or general impairment of digestive vacuole function, as contributors to this peptide phenotype.

In response to perturbations within the digestive vacuole and impaired Hb catabolism, we propose that the parasite engages an ultimately futile compensatory mechanism that increases the abundance and activity of all proteases involved in Hb digestion, except falcilysin (Fig 4A). Falcilysin has been shown to localise to both the parasite apicoplast and the digestive vacuole, suggesting that it may have a function beyond Hb catabolism [56, 57]. The activity of cysteine proteases involved in Hb digestion was elevated within 1 h of ozonide exposure, before the first time point of significant small peptide depletion (1.5 h), indicating that increasing Hb protease capacity may allow the parasite to successfully compensate for disrupted Hb digestion for a short period. Alternatively, the rapid peroxide effect on Hb catabolism may occur before there is a detectable change in small peptide levels using metabolomics.

Rapid disruption of Hb catabolism by the ozonides (and artemisinins) agrees with the hypothesis that peroxide-based drugs are activated by Fe(II) or haem to produce reactive intermediates in the parasite digestive vacuole where Hb digestion takes place. The resulting ozonide-derived radicals were recently shown to alkylate haem within iRBCs after short drug exposures [58] and the radicals may also alkylate and inactivate digestive vacuolar proteins, including the proteases involved in Hb digestion [19, 20, 27]. Digestive vacuole FPs play an important role in Hb degradation [33]. The activity of these enzymes increased after ozonide treatment (Fig 4B), and cysteine protease inhibition with E64d resulted in accumulation of full-length Hb and digestive vacuole swelling, whereas these features were not seen in peroxide treated-parasites (S6 Fig). These findings suggest that the digestive vacuole FPs are unlikely to be the Hb proteases initially inactivated by the ozonides, and this may be important therapeutically as functional FPs are essential for peroxide antimalarial activity [28, 30, 52, 59]. Indeed, ozonides (and artemisinins) are reported to alkylate a range of proteins localised to the parasite digestive vacuole, including other proteases involved in Hb digestion, for example, plasmepsins [19, 20, 27], which could be the initial intraparasitic protein targets important for peroxide antimalarial activity. Consistent with our hypothesis that disrupted Hb catabolism is the key early event initiated by peroxide treatment, we demonstrated that the initial antiparasitic effects of peroxide exposure were enhanced when parasites were forced to rely solely on Hb degradation for amino acids (Fig 4E). Taken together, we propose that Hb digestion is the initial pathway affected as a result of peroxide antimalarial treatment, however, the precise molecular mechanism responsible for altered Hb catabolism remains unclear.

Depletion of short Hb-derived peptides following peroxide treatment was also confirmed in artemisinin resistant (Cam3.II^{R539T}) and sensitive (Cam3.II^{rev}) parasite lines (Fig 2D) that exhibit differential sensitivity to ozonides and DHA in the *in vitro* ring-stage survival assay [30, 31, 60]. It should be noted that there are conflicting reports on the activity of ozonides against parasite strains with reduced artemisinin sensitivity in the *in vitro* ring-stage survival assay and this appears to be dependent on the ozonide and K13 mutation tested [60–62]. We found that the level of drug-induced peptide depletion was generally less extensive in the *K13*-mutant (Cam3.II^{R539T}) compared to that in the drug-treated *K13*-wildtype revertant strain (Cam3.II^{rev}) (Fig 2D), suggesting that both ozonides and DHA have diminished impact on Hb catabolism in resistant parasites, supporting the hypothesis that *in vitro* cross-resistance exists between artemisinins and ozonides in parasites with a R539T mutation. The diminished drug effect on Hb catabolism may be a result of increased survival of *K13*-mutants following short peroxide exposure and could be mediated by altered Hb metabolism [37, 63, 64], augmented antioxidant defence pathways [37, 65, 66] or an enhanced stress response [32].

One caveat is that the precise origin of the depleted di, tri and tetrapeptides detected by untargeted metabolomic screening cannot be definitively determined due to their short sequences. MS/MS confirmation of the amino acid sequence was obtained for a subset of these depleted peptides and the confirmed sequences could be mapped to Hb. Furthermore,

combined with additional lines of evidence pointing to a mechanism involving ozonide-induced disruption of Hb catabolism, it is likely that most of the small peptides that were perturbed by drug treatment originated from Hb. The short peptides unable to be mapped to Hb could originate from other RBC proteins or *Plasmodium* proteins, and could be associated with peroxide-induced inhibition of proteasome function and altered proteostasis [21]. It is important to note that the majority of peptides detected in the metabolome were not perturbed by drug treatment and most of these unaffected peptides could not be mapped to Hb. Furthermore, endogenous long peptides from only one *Plasmodium* protein were reproducibly perturbed by peroxide treatment. These data suggested that general parasite protein degradation was not significantly affected as a result of these short peroxide exposures.

Extended drug treatment (> 3 h) induced disruption of additional biochemical pathways beyond Hb catabolism, including lipid and nucleotide metabolism (Fig 6A), representing secondary biochemical pathways involved in peroxide activity. In both ring and trophozoite-stage parasites, drug treatment induced an accumulation of several metabolic intermediates in the *de novo* synthesis pathways of PC and PE lipids (known as the Kennedy Pathways) (Fig 6B and S12 and S14 Figs), which are the major lipid components of parasite membranes [45]. Proteomic analysis revealed that all enzymes directly upstream of the elevated metabolites in the Kennedy Pathways were also increased in abundance (Fig 6B and S13 Fig), possibly to increase the synthesis of PC and PE as a biochemical response to drug-induced membrane damage. These findings are consistent with the biological activity of ozonides and artemisinins involving non-specific damage to parasite membranes, such as the digestive vacuole and mitochondrial membranes [67, 68], through lipid peroxidation, which becomes apparent after an extended duration of drug exposure (> 3 h) and the production of reactive oxygen species [67, 69–72]. Inhibiting the synthesis of key phospholipids is detrimental to parasite survival [73] and it is likely that perturbation to this pathway contributes to peroxide antimalarial activity.

Prolonged ozonide and DHA exposure in trophozoite-stage parasites also led to the depletion of DGs and TGs (Fig 6B and S12 Fig). These are the two main neutral glycerolipid species in parasites [74] and these lipids increase in abundance as the asexual parasite matures, indicating their importance for growth and development [74]. DGs and TGs are packaged into neutral lipid bodies, which are closely associated with the parasite digestive vacuole [75–77]. Neutral lipid bodies are thought to concentrate free haem and catalyse its biocrystallisation into non-toxic haemozoin [76–78], placing them proximal to the location where peroxide antimalarials are thought to be activated. Furthermore, fluorescently-tagged artemisinin and ozonide derivatives have been shown to accumulate in neutral lipid bodies [70, 71]. Activated drug, or potentially alkylated haem adducts [58], may therefore promote oxidative damage to DGs and TGs within neutral lipid bodies and limit the availability of key neutral lipids that are required for parasite development [74]. As DGs are key precursors for membrane phospholipid synthesis (e.g. PC and PE), it is expected that DG depletion also contributes to the upregulation of *de novo* phospholipid biosynthesis (Kennedy) pathways.

Disruption of the parasite pyrimidine biosynthetic pathway at both the metabolite and protein levels (Fig 6C and S15 and S16 Figs) was also apparent in ozonide and DHA treated parasites. This finding is consistent with previous studies demonstrating DHA-induced alterations in parasite pyrimidine metabolism [45]. Furthermore, carbamoyl phosphate synthetase and aspartate carbamoyl transferase, which catalyse the initial steps of parasite pyrimidine biosynthesis, are reported to be alkylation targets of artemisinins, although this has not yet been shown for the ozonides [19]. Peroxide-induced inhibition of one or both of these initial pyrimidine biosynthetic enzymes may be responsible for the depletion of downstream pyrimidine biosynthesis intermediates, and a corresponding increase in the protein levels of some enzymes in this pathway as a compensatory response, as shown in our study.

The alternative hypothesis that these secondary pathways are non-specific responses in dying parasites is also possible. However, different drug-specific biochemical responses were reported in metabolomics, proteomics and peptidomics studies of other antimalarials, including the 4-aminoquinolines that target the digestive vacuole via a different mechanism, and even when parasites were exposed to drugs for extended durations [45–47, 79, 80]. Combined with reports showing that peroxide antimalarials target proteins in both the phospholipid and pyrimidine biosynthesis pathways [19, 20, 27] and colocalise with neutral lipids within iRBCs [70, 71], the drug-specific biochemical responses of parasites detected in metabolomics studies suggests that the secondary metabolic alterations observed here are likely ozonide-specific and related to the pleiotropic effect of peroxides on parasite metabolism.

Our work demonstrating that peroxide antimalarials affect multiple aspects of parasite biochemistry is consistent with previous reports [45, 46]. Global proteomic analysis of ozonide and DHA-treated parasites revealed a pronounced enrichment of proteins involved in protein translation and the ubiquitin-proteasome system (Fig 5 and S11 Fig). Previous studies have shown that artemisinins inhibit protein translation and proteasome activity [21, 81], and the observed enrichment in these pathways from our study may represent a response to this inhibition, either by regulation of protein expression, or decreased degradation of these proteins. Furthermore, the enrichment of proteins in the translation and proteasomal pathways may reflect a general stress response to enhance protein turnover and mitigate peroxide-mediated cellular damage [82]. Peroxide-induced oxidative insult and widespread protein alkylation is thought to induce accumulation of damaged and misfolded proteins [22, 32, 83], and the parasite relies on translational regulation and a functional ubiquitin-proteasome system to restore proteostasis [84, 85].

Based on our findings, we have proposed a model for the MoA of peroxide antimalarials (Fig 7). Hb-derived free haem activates the peroxide bond of ozonides (or artemisinins) within the digestive vacuole and the resulting drug-derived radicals initially alkylate haem [58] and damage proteases involved in Hb digestion leading to disruption of the Hb degradation pathway. In a futile response to drug-induced damage, the parasite increases the levels of Hb-digesting proteases to restore normal Hb catabolism. Following prolonged exposure, drug-derived radicals induce further oxidative insult and cause widespread alkylation of parasite components, including damage to lipids, and proteins involved in other vital parasite functions. To mitigate drug-induced cellular damage, the parasite engages a proteostatic stress response involving upregulation of proteins involved in translational regulation and the ubiquitin-proteasome system. Parasite death ultimately occurs when drug-mediated damage overwhelms these parasite defensive mechanisms. In artemisinin resistance, *K13* mutations alter parasite Hb metabolism [37, 63, 64] and enhance antioxidant capacity [37, 65, 66] and stress response pathways [32], limiting the damage of drug-derived radicals and increasing parasite survival.

Although DHA had a more rapid and pronounced effect on metabolism compared to the ozonides, these antimalarials affected similar biochemical pathways suggesting that they have a similar MoA. This could raise concerns for the deployment of ozonides in areas affected by artemisinin resistance [86], which is characterised by infections with parasites that can withstand the short DHA exposures observed in the pharmacokinetics of clinically-used artemisinins [17, 30]. However, the temporal metabolomics analysis demonstrated that prolonged peroxide exposure perturbed additional pathways beyond the digestive vacuole, raising the possibility that long half-life ozonides (e.g. OZ439) may impact additional parasite functions during prolonged exposure, and potentially overcome resistance associated with the short-lived artemisinins. There are mixed reports regarding ozonide activity in artemisinin resistant parasites, and further clinical studies are required to determine the potential utility of ozonides

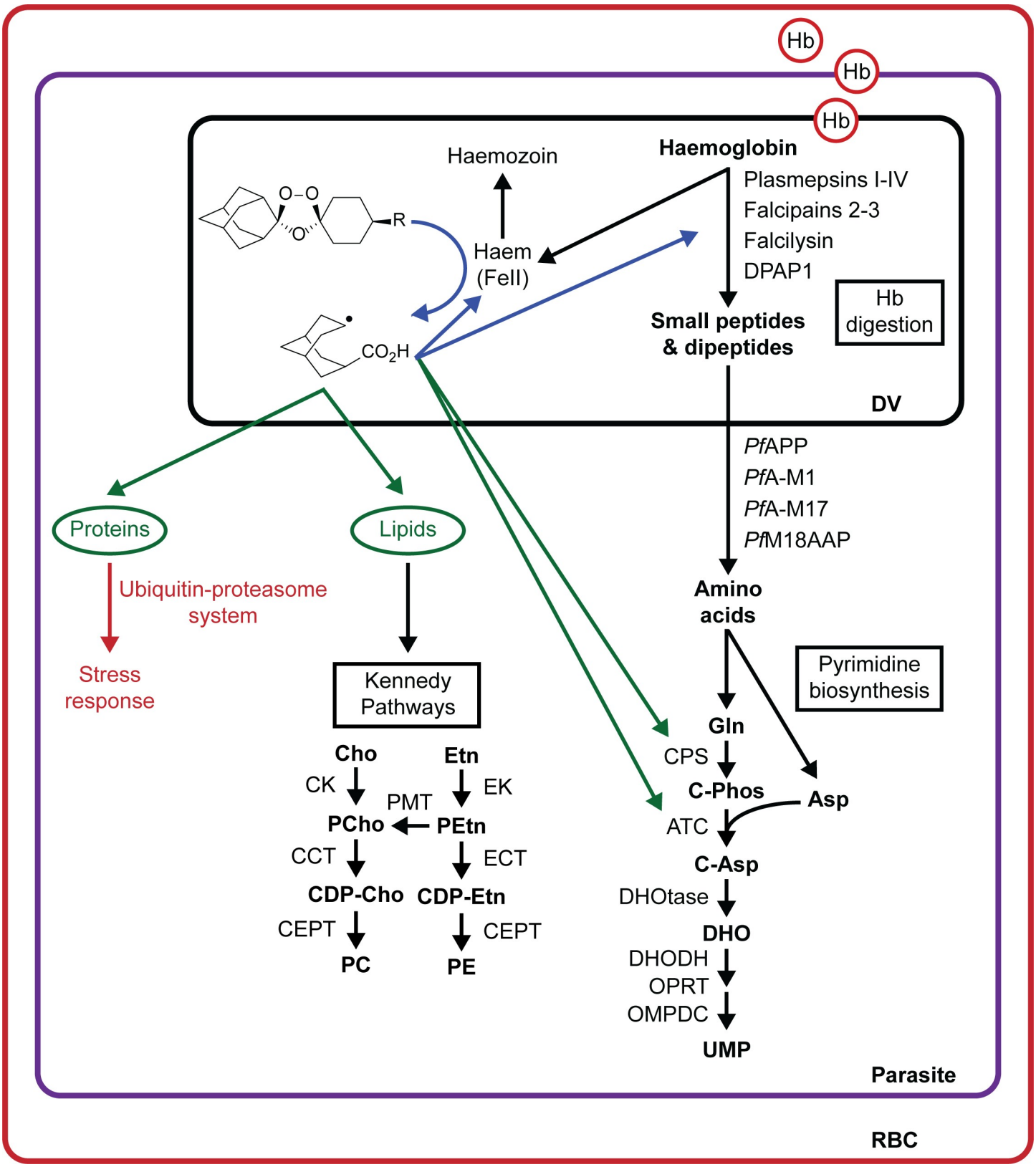


Fig 7. Proposed model for ozonide antimalarial activity in *P. falciparum* infected red blood cells. Haemoglobin-derived haem activates peroxide antimalarials within the parasite digestive vacuole. The resulting drug-derived radicals initially damage components proximal to the activation site, including proteases involved in

haemoglobin digestion (arrow shown in blue). This leads to disruption of the haemoglobin degradation pathway. To correct for peroxide-induced damage, parasites may respond by increasing the levels of proteases involved in haemoglobin catabolism. Peroxide radicals induce further oxidative insult and cause widespread alkylation of parasite components as the duration of drug exposure is increased (arrows shown in green). This may include damage to lipids, inducing upregulation of the Kennedy Pathways, and proteins involved in other vital parasite functions, such as pyrimidine biosynthesis. To mitigate peroxide-induced cellular damage, the parasite engages a stress response involving translational regulation and the ubiquitin-proteasome systems. Asp, aspartic acid; ATC, aspartate carbamoyltransferase; C-Asp, carbamoyl-aspartate, C-Phos, carbamoyl-phosphate; CCT, choline-phosphate cytidyltransferase; CDP-, cytidine-diphospho-; CEPT, choline/ethanolamine phosphotransferase; Cho, choline; CK, choline kinase; CMP, cytidine monophosphate; CPS, carbamoyl phosphate synthetase; DHO, dihydroorotate; DHODH, dihydroorotate dehydrogenase; DHOtase, dihydroorotase; DV, digestive vacuole; ECT, ethanolamine-phosphate cytidyltransferase; EK, ethanolamine kinase; Etn, ethanolamine; Gln, glutamine; Hb, haemoglobin; OMPDC, orotodine 5'-phosphate decarboxylase; OPRT, orotate phosphoribosyltransferase; PC, phosphatidylcholine; PE, phosphatidylethanolamine; PCho, choline phosphate; PEtn, ethanolamine phosphate; PMT, phosphoethanolamine N-methyltransferase; RBC, red blood cell; UMP, uridine monophosphate.

https://doi.org/10.1371/journal.ppat.1008485.g007

in artemisinin resistant malaria infections [58]. In the context of growing concerns about the spread of multi-drug resistant malaria parasites, this insight into the MoA of peroxide antimalarials, and the parasite's response to treatment, offers potential avenues for targeting the malaria parasite with novel drug regimens that have improved antimalarial efficacy and limit the generation of drug resistance.

Materials and methods

Plasmodium falciparum culture conditions

P. falciparum parasites (3D7 strain, Cam3.II^{R539T}, and Cam3.II^{rev}) were cultured as previously described [87]. RBCs were obtained from the Australian Red Cross Blood Service in Melbourne. Artemisinin resistant and sensitive *P. falciparum* isolates were kindly provided by Professor David Fidock, Columbia University and included the field-derived *K13*-mutant, Cam3.II^{R539T}, and the *K13*-wildtype on an isogenic background (Cam3.II^{rev}) [31]. Parasites were tightly synchronised by double treatment with sorbitol [88]. For 3D7 parasites, trophozoite or ring stage parasite cultures were adjusted to 10% parasitaemia and 2% Hct. For experiments using artemisinin resistant and sensitive isolates, trophozoite parasite cultures were adjusted to 4% parasiteamia and 2% Hct.

Metabolomics sample preparation

In 3D7 parasites, a comprehensive time-course analysis was performed to determine the peroxide-induced metabolic profile in ring- and trophozoite-stage parasites. Ring-stage parasite cultures (6–12 h post invasion) were exposed to drug (1 μM of OZ277 or OZ439, 300 nM of DHA and 0.03% DMSO) for 0, 3, 6 and 9 h prior to metabolite extraction, while trophozoite stage parasite cultures (28–34 h post invasion) were exposed to drug (300 nM of OZ277 or OZ439, 100 nM of DHA and $<$ 0.03% DMSO) for 0, 0.5, 1.5, 3, 6 and 9 h.

In artemisinin resistant and sensitive isolates, prior to drug incubation, the age of paired artemisinin sensitive and resistant parasites was confirmed by analysis of Giemsa stained thin blood smears. Trophozoite parasite cultures (22–26 h) were exposed to 100 nM of DHA, OZ277 and OZ439 nM for a duration of 1, 3 and 5 h, respectively. Under the conditions used in this metabolomics study (4% parasitaemia and 2% Hct), these concentrations were found to be sub-lethal in both the Cam3.II^{R539T} and Cam3.II^{rev} parasite lines ($<$ 50% loss of viability for DHA and OZ277 after a 1 h and 3 h pulse, respectively, and $<$ 40% loss of viability for OZ439 after a 3 h pulse). Metabolomics studies included treatment of non-infected RBCs as controls and all experiments were performed on at least three independent occasions.

Following drug incubation, for ring-stage experiments (3D7), metabolites were extracted from 2 x 10^8 cells using 200 μL of cold chloroform/methanol/water (1:3:1), while for trophozoite stage experiments (3D7), 1 x 10^8 cells were used and metabolites extracted using 150 μL of cold chloroform/methanol/water (1:3:1). For trophozoite stage experiments (3D7) where long-

term peroxide treatment was used (up to 9 h), metabolites were extracted from 1 x 10^8 cells using 150 μL of cold methanol. For artemisinin resistant and sensitive isolates, 1 x 10^8 cells were used and metabolites extracted using 150 μL of cold methanol. Metabolomics extraction was as previously described [46]. Insoluble precipitates were removed by centrifugation and 110 μL of metabolite extract was transferred to glass LC-MS vials and stored at -80˚C until analysis. A 15 μL aliquot of each sample was combined to generate a pooled biological quality control (PBQC) sample for analytical quality control and metabolite identification procedures.

Untargeted metabolomics LC-MS analysis and data processing

To measure the metabolic perturbations induced by peroxide antimalarials in iRBCs and infer the major pathways affected by treatment we employed an untargeted approach. Untargeted analyses profile all detectable metabolite signals within a biological system, can be employed without existing knowledge of a putative drug target and are particularly useful when multiple targets might be involved in drug action. In contrast, targeted metabolite analyses are hypothesis-driven experiments that are more suited when the mode of action of an antimalarial is suspected and measures drug-induced changes to a predefined subset of metabolites, often restricted to a particular metabolic pathway [89].

Untargeted LC-MS analysis was performed using HILIC chromatography (ZIC-pHILIC; Merck) with an alkaline mobile phase on an Ultimate U3000 LC system (Dionex) and Q Exactive Orbitrap MS (ThermoFisher) operating in both positive and negative ion mode as previously described [37, 46]. The PBQC sample was run periodically throughout each LC-MS batch to monitor signal reproducibility and support downstream metabolite identification. Extraction solvent was used as blank samples to identify possible contaminating chemical species. To aid in metabolite identification, approximately 250 authentic metabolite standards were analysed prior to each LC-MS batch and their peaks and retention time manually checked using the ToxID software (Thermofisher).

Metabolomics data were analysed using the IDEOM workflow [90]. High confidence metabolite identification (MSI level 1) was made by matching accurate mass and retention time to authentic metabolite standards [91]. Putative identifications (MSI level 2) for metabolites lacking standards were based on exact mass and predicted retention times [92]. Specifically, the identification of peptides was based on either accurate mass or a combination of accurate mass and MS/MS analysis, which allowed definitive confirmation of the amino acid sequence in selected peptides. In the ring and artemisinin resistance studies, LC-MS peak heights representing metabolite abundances were normalised by median peak height, while quality control procedures indicated that normalisation of metabolite abundances was not required in the 3D7 trophozoite studies. Univariate statistical analysis was performed using IDEOM and Welch's *t* test [90]. Multivariate statistical analysis was performed on the mean centred and auto-scaled data using the web-based tools in Metaboanalyst [93]. Sparse partial least squares–discriminant analysis (sPLS-DA) algorithms were run with increasing numbers of metabolites in each component (up to 150 metabolites), with minor changes to the model when more than 10 metabolites were used. The final sPLS-DA plots shown in the supplementary data were developed using 10 metabolites in each component. Significant metabolites (P-value ≤ 0.05) were confirmed by manual integration of raw LC-MS peak areas in TraceFinder (ThermoFisher).

Functional assays to measure haemoglobin abundance

The Hb fractionation assay was adapted from [35, 80]. Briefly, 3D7 trophozoite-stage parasites were incubated with DHA, OZ277, OZ439, E64d or a DMSO control for either 1 or 3 h.

Following incubation, Hb, haem and haemozoin species were separated and measured using the Hb fractionation assay [35, 80], and smears were made using Giemsa stain to check for parasite viability and digestive vacuole morphology by light microscopy. For the Hb fractionation assay, the samples were normalised via a paired analysis to the DMSO control and graphed as their fold change vs DMSO ± SD. All fractions had >4 replicates from >2 independent experiments.

Hb monomer was also measured using SDS-PAGE gel. Briefly, 3D7 trophozoite-stage parasites were incubated with OZ277, E64d or a DMSO control for 3 h. Following incubation, extracted parasites were resolved on SDS-PAGE gels and proteins stained using Coomassie blue.

Peptidomics sample preparation

Peptidomics samples were prepared as previously described with minor modifications [37]. Briefly, intracellular parasites were harvested after 3 h of drug treatment followed by trichloroacetic acid protein precipitation and centrifugal filtration using a 10 kDa cut-off filter (Amicon Ultra). The flow-through containing endogenous peptides was collected and peptide concentration was measured using a bicinchoninic acid (BCA) protein assay (Thermo Scientific Pierce) as per manufacturer's protocol. Equal concentration of peptides (53–75 μg) were used for peptidomic analysis. Peptide samples were then subjected to desalting using in-house generated C18 StageTips [94]. The elutes were then dried and resuspended in 20 μL of 2% (v/v) acetonitrile (ACN) and 0.1% (v/v) formic acid (FA) for LC-MS/MS analysis.

Peptidomics nanoLC-MS/MS analysis and data processing

LC-MS/MS analysis was performed using an Ultimate U3000 Nano LC system (Dionex) and Q Exactive Orbitrap MS (ThermoFisher) as previously described [37].

Peptide identification was performed using PEAKS DB software [95]. Maximum mass deviation and false discovery rates were set at 0.5 Da and 0.01 respectively. No post translational modification or digestion were selected and identified peptide sequences were matched to *Homo sapiens* and *P. falciparum* databases. The mass to charge ratio and retention time of each identified peptide were imported into TraceFinder (ThermoFisher) and the peak intensity for each peptide was obtained manually. Further statistical analyses (Student's *t* test) were performed using Microsoft Excel for paired drug treated and DMSO control samples.

Proteomics sample preparation and triplex stable isotope dimethyl labelling

Proteomics samples were prepared as previously described with minor modifications [37]. Briefly, 1000 μg of protein, accurately determined using Pierce BCA assay, from each sample was incubated overnight with sequencing grade trypsin (Promega) (1:50) at 37˚C. Quantitative triplex stable isotope dimethyl labelling was initiated on the following day using light, intermediate or heavy dimethyl labelling reagents [96]. The samples were then subjected to ion-exchange fractionation using a disposable Strong Cationic Exchange Solid Phase Extraction cartridge (Agilent Bond Elut) [97]. The fractions were desalted using in-house generated StageTips [94], dried and resuspended in 20 μL of 2% (v/v) ACN and 0.1% (v/v) FA for LC-MS/MS analysis.

Proteomics nanoLC-MS/MS analysis and data processing

LC-MS/MS analysis was performed using an Ultimate U3000 Nano LC system (Dionex) and Q Exactive Orbitrap MS (ThermoFisher) as previously described [37]. Protein identification and quantification was performed using the MaxQuant proteomics software [98]. The data analysis parameters in MaxQuant were set as previously described [37] with minor

modifications. Dimethylation settings were adjusted to triplets; DimetNterm0 with DimetLys0, DimetNterm4 with DimetLys4 and DimetNterm8 with DimetLys8 were selected as light, intermediate and heavy label respectively. To correct for differences in protein amount between groups, the protein ratios were normalised in MaxQuant at the peptide level so that the log2 ratio is zero [98]. Known contaminants such as trypsin, keratin and reverse sequences were removed from the MaxQuant output. Fold-changes for the drug treated samples relative to the DMSO control samples were calculated in Microsoft Excel. One sample t-test was used to test the mean of combined experiment groups against the known mean ($\mu = 0$) [99]. For each drug, the proteins that were identified in at least three independent experiments were filtered based on P-value (≤ 0.05) and fold-change (≥ 1.5) to generate a list of significantly perturbed proteins. The bioinformatics interaction network analysis tool STRINGdb [100] was used to build a protein-protein interaction network using the significantly perturbed proteins. Connectivity was based on experimental, database and co-expression evidence and a strict minimum interaction score (> 0.7) was applied to limit false positive associations in the predicted network. The STRINGdb protein connectivity output was exported to Cytoscape 3.6 [101] and the ClusterONE algorithm was used to integrate and visualise relationships between proteins that were significantly perturbed by drug treatment.

Temporal activity-based protein profiling of cysteine protease activity using activity-based probes

Activity-based probes (ABPs) were used to measure protease activity [42] following ozonide exposure according to established methods [102]. In these assays, tightly synchronised trophozoite stage parasites (28–34 h post invasion, 10% parasitaemia and 2% Hct) were treated with OZ277 (300 or 1000 nM) or OZ439 (300 nM) for up to 5 h. Untreated parasite controls contained an equivalent volume of DMSO ($< 0.01\%$). Following ozonide treatment, parasites were purified by lysing the red blood cells using 0.1% saponin on ice. Parasite pellets were then lysed by sonication in citrate buffer (50 mM trisodium citrate [pH 5.5], 0.5% CHAPS, 0.1% Triton X-100, 4 mM dithiothreitol) or phosphate buffered saline (PBS) (pH 7.2). Supernatants were then cleared by centrifugation and transferred to new tubes. Protein concentration in each sample was determined using BCA protein assay (Pierce) and an equal amount of each sample was incubated with ABPs (DCG04; 2 μM or FY01; 1 μM) for 30 min at 37˚C to label active cysteine proteases. In experiments including the reversible cysteine protease inhibitor N-acetyl-Leu-Leu-Norleu-al (ALLN) (Merck), parasite lysates were pre-incubated with 10 μM of the inhibitor for 30 min prior to addition of the ABP for a further 15 min. In all cases, the reaction was quenched by the addition of 5x reducing buffer (50% glycerol, 250 mM Tris-Cl [pH 6.9], 10% SDS, 0.05% bromophenol blue, 6.25% beta-mercaptoethanol), boiled and separated by sodium dodecyl sulfate polyacrylamide (SDS-PAGE) on 15% polyacrylamide gels. As DCG04 is biotin-tagged, proteins were transferred to nitrocellulose membranes and incubated with streptavidin-AlexaFluor-647 followed by fluorescence detection with a Cy5 filter (excitation/emission: 649/670 nm) with an Amersham Typhoon 5 Biomolecular Imager (GE Healthcare Life Sciences). FY01 contains a Cy5 fluorophore, thus visualization of its targets was achieved by direct scanning of the gel for Cy5 fluorescence. Coomassie staining was used to confirm equal protein loading. Images were processed and quantified in either ImageJ 1.51f or Adobe Photoshop Creative Cloud 2017.

Determination of antimalarial potency on parasites cultured in complete RPMI medium or medium lacking exogenous amino acids (except isoleucine)

Full RPMI medium 1640 (Sigma-Aldrich) contained all 20 amino acids and was supplemented with 5.94 g/l HEPES, 2.1 g/l $NaHCO_3$, 50 mg/l hypoxanthine and 5 g/l Albumax II (Lifetech),

making AA medium. RPMI medium 1640 lacking all amino acids (Life Research) was supplemented with isoleucine (Sigma-Aldrich) at a final concentration of 147.5 μM to make Iso medium [43]. All other supplements (HEPES, $NaHCO_3$, hypoxanthine and Albumax II) were added as for AA medium above. To examine parasite susceptibility to the peroxide antimalarials in the Iso and AA mediums, drug pulse activity assays were performed as previously described [103]. Briefly, the medium of iRBC cultures containing 30 h trophozoite-stage parasites (10% parasitaemia and 2% Hct) was replaced with either Iso or AA medium immediately before initiating drug treatment. Parasites were treated with 300 nM of pyrimethamine, OZ277 or OZ439 or 100 nM of DHA for 3 h. Following the incubation period, drugs were removed by washing the cultures as previously described [28] using either AA or Iso medium supplemented with 2–5% Albumax II. Cultures were then adjusted to 0.5% parasitaemia and 2% Hct (final volume, 200 μL) as previously described [28] with either Iso or AA medium. After 48 h the parasitaemia was measured by counting Giemsa stained thin blood smears. Parasite survival was determined by graphing the parasitaemia for each test compound relative to the appropriate untreated medium (Iso or AA) control, which was set to 100%. All assays were performed in triplicate in at least three independent experiments.

Supporting information

S1 Fig. Integrative multi-omics (metabolomics, peptidomics and proteomics) and activity-based protein profiling (ABPP) workflows for the comprehensive analysis of peroxide antimalarial action in *P. falciparum* infected red blood cells (RBCs). Metabolomics (green boxes) samples were extracted from infected RBCs at regular intervals (up to 9 h after drug addition) and the extracted samples were analysed by LC-MS and processed using IDEOM. For peptidomics (blue boxes), endogenous peptides were extracted from saponin-lysed parasites, samples were subjected to 10 kDa cut-off centrifugal filtration and then an equal amount of peptides were used for analysis by nanoLC-MS/MS before data was processed using PEAKS software. Protein pellets following trichloracetic acid (TCA) precipitation were collected for proteomic sample preparation (brown boxes). Equal amount of proteins were digested using trypsin, labelled using dimethyl labelling to allow differential quantitative proteomic analysis and examined using nanoLC-MS/MS followed by data processing using MaxQuant. ABPP assays (red boxes) were performed by selectively labelling active cysteine proteases in the parasite lysate using various activity-based probes (ABPs), then visualising protease activity in a gel-based format.
(TIF)

S2 Fig. Metabolic perturbations in trophozoite stage parasite cultures. a, Percentage of significantly perturbed metabolites (Welch's *t* test; P-value < 0.05 and fold change ≥ 1.5) following exposure to increasing durations of OZ277 (blue), OZ439 (green) and DHA (red) (0.5, 1.5 and 3 h). **b**, Pathway enrichment analysis showing the percentage of significantly perturbed metabolites (Welch's *t* test; P-value < 0.05 and fold change > 1.5) as a function of metabolite class for short (0.5, 1.5 and 3 h) exposure with OZ277, OZ439 (both 300 nM) and DHA (100 nM).
(TIF)

S3 Fig. Peroxide-induced metabolic perturbations in ring-stage parasite cultures. a, Percentage of significantly perturbed metabolites (Welch's *t* test; P-value < 0.05 and fold-change > 1.5) at each time point (0, 3, 6 and 9 h) following OZ277 (blue), OZ439 (green) and DHA (red) treatment of ring-stage infected cultures. **b**, Heatmap showing the average fold change for all identified peptides at each time point after OZ277, OZ439 and DHA treatment

in ring-stage parasites. For each time point, values represent the average of four independent biological replicates, expressed relative to the average untreated control value for that respective time point.
(TIF)

S4 Fig. Multivariate analysis of peroxide-induced perturbations in ring-stage parasite cultures. a-**c**, Sparse partial least squares–discriminant analysis (sPLS-DA) of the metabolomics data for ring-stage parasite infected RBCs treated with peroxide antimalarials for 3 h (**a)**, 6 h (**b),** and 9 h (**c**).
(TIF)

S5 Fig. Peroxide-induced alterations in peptide abundance in Cam3.II^{rev} and Cam3.II^{R539T} parasite lines. a, Heatmap of differentially abundant peptides (altered $\geq$ 1.5-fold relative to the untreated control) in artemisinin-resistant Cam3.II^{R539T} and artemisinin-sensitive Cam3.II^{rev} parasite lines following peroxide treatment. Data shown are the average for three or five biological replicates expressed relative to the average for the untreated control from the sensitive parasite line (DMSO, Cam3.II^{rev}).**b**, Sequence coverage for putative haemoglobin (Hb)-derived peptides that were altered in abundance following peroxide antimalarial treatment relative to the untreated control. All peptides, except TT and SK (or its isomers) were reduced in abundance in treated parasites compared to control levels. The solid black bars represent peptide sequences that were confirmed by MS/MS analysis and the dashed bars represent putative peptide sequences. For putative peptide sequences, all potential isomers have been mapped.
(TIF)

S6 Fig. Peroxide-induced alterations in haemoglobin abundance in 3D7 parasite lines. a, A panel of representative giemsa stained parasites treated with 300 nM of OZ277 or OZ439, 100 nM of DHA, a DMSO negative control or a 27 μM E64d positive control for a swollen digestive vacuole after 1 h and 3 h. **b**, Bar charts representing the relative levels of haemoglobin, free heme and hemozoin in trophozoite-stage parasites following either a 1 or 3 h incubation with 300 nM of OZ277 and OZ439, 100 nM of DHA or 27 μM of E64d expressed as the fold change when compared to a DMSO control. Bars represent the mean of >4 paired replicates from at least two independent experiments with the error bars expressed as SD. **c**, SDS-PAGE gel image of haemoglobin monomer band following treatment with OZ277 (300 nM for 3 h), E64d (27 μM for 3 h) and DMSO control. **d**, Haemoglobin α and β abundance measured using quantitative proteomics for treated parasites (100 nM DHA, 300 nM OZ277 and OZ439 for 3 h), values are the average fold change (± SD) relative to the untreated control of at least three biological replicates.
(TIF)

S7 Fig. Volcano plot showing the global proteomic changes associated with peroxide antimalarial treatment of trophozoite-stage parasite cultures. Proteins identified in at least three independent experiments following treatment of trophozoite stage parasites with OZ277 (1293 proteins, indicated by blue colour dots), OZ439 (1284 proteins, green dots) and DHA (1613 proteins, red dots). Trophozoite infected cultures were incubated with OZ277, OZ439 (both 300 nM) or DHA (100 nM) for 3 h. Proteins above the significance threshold (P-value $\leq$ 0.05) and outside the grey shaded area (fold change $\geq$ 1.5) were considered significant.
(TIF)

S8 Fig. Activity-based protein profiling of parasite cysteine protease activity after peroxide treatment using the activity-based probe (ABP), DCG04 under neutral pH conditions. a, Cysteine protease activity and densitometric analysis of the DPAP1 and FP 2/3 signal after OZ277 and OZ439 treatment in *P. falciparum* trophozoite-stage parasites using DCG04 at pH 7.2 (neutral). Live parasites were treated for 1, 3 or 5 h with OZ277, OZ439 or DMSO (control) in 3–4 independent experiments and the saponin lysates were labelled with DCG04 to determine cysteine protease activity. DCG04 labelling was detected by blotting membranes with streptavidin-AF647 after SDS-PAGE and transfer. The lanes for each time point are independent drug treatments and represent at least three biological replicates per time point that were run on the same gel side-by-side. Densitometric analysis is shown relative to the untreated control at the corresponding time point (±SD). **b**, ALLN inhibition of cysteine protease activity under neutral (pH 7.2) and acidic (pH 5.5) conditions. Live parasites were treated for 3 h with OZ277, OZ439 or DMSO (control) and the saponin lysates were pre-incubated with (+) or without (-) the cysteine protease inhibitor ALLN (10 μM for 30 min) prior to labelling with DCG04.
(TIF)

S9 Fig. Activity-based protein profiling of parasite cysteine protease activity after peroxide treatment using the activity-based probe (ABP), FY01. a-b, SDS-PAGE gel showing parasite cysteine protease activity after OZ277, OZ439 and DMSO (control) treatment in trophozoite-stage parasites using the FY01 probe, at pH 5.5 (acidic) (**a**) and pH 7.2 (neutral) (**b**). Live parasites were treated for 1, 3 or 5 h in 3–4 independent experiments. Treated parasites were saponin lysed and labelled with FY01 to determine cysteine protease activity. Proteins were resolved by SDS-PAGE and the gel was scanned for Cy5 fluorescence to detect probe labelling. For (a) and (b) the lanes for each time point are independent drug treatments and represent at least three biological replicates per time point that were run on the same gel side-by-side. < Unidentified bands.
(TIF)

S10 Fig. *P. falciparum* parasite sensitivity to 48 h of OZ277 treatment when cultured in complete (AA) and isoleucine alone (Iso) medium. Trophozoite-stage parasites at 1% parasitaemia and 2% haematocrit cultured in either medium containing all amino acids (AA, black line) or isoleucine alone medium (Iso, grey line) were incubated with different concentration of OZ277 for 48 h and the 50% inhibitory concentration (IC_{50}) determined using the SYBR green assay. The IC_{50} (nM) for OZ277 in parasites cultured in AA medium was 6.3 ± 1.6. The IC_{50} (nM) for OZ277 in parasites cultured in Iso medium was 6.6 ± 1.1. IC_{50} results are the mean and standard deviation of three biological repeats. A representative growth curve is shown.
(TIF)

S11 Fig. Network analysis of parasite proteins perturbed following treatment with DHA. The network analysis was built using the STRINGdb interaction network analysis output (connectivity was based on experimental, database and co-expression evidence with a minimum interaction score of 0.7) in Cytoscape 3.6 with the ClusterONE algorithm. Node size represents P-value and node colour represents fold-change from at least three independent replicates.
(TIF)

S12 Fig. Peroxide-induced perturbations to lipid metabolism in trophozoite-stage parasite cultures. a, Heatmap showing the average fold change for all identified lipids and lipid metabolites at each time point after prolonged exposure to OZ277, OZ439 and DHA in trophozoite-stage *P. falciparum* parasites. Values represent the average of three biological replicates,

expressed relative to the average untreated control value for that respective time point. **b**, *De novo* synthesis pathways for phosphatidylcholine (PC) and phosphatidylethanolamine (PE) in *P. falciparum*. Metabolites in red and blue were increased and decreased in abundance after drug treatment respectively. Enzyme names are shown in solid boxes. The dashed arrow represents an alternative route for the synthesis of PC from ethanolamine (Etn) in *P. falciparum*. **c**, Pathways for the synthesis of phospholipids and triglycerides from phosphatidic acid precursors. CCT, choline-phosphate cytidyltransferase; CDP-, cytidine-diphospho-; CEPT, choline/ethanolamine phosphotransferase; Cer, ceramide; Cho, choline; CK, choline kinase; CMP, cytidine monophosphate; DAG/DG, diglyceride; DM-, dimethyl-; ECT, ethanolamine-phosphate cyitidyltransferase; EK, ethanolamine kinase; Etn, ethanolamine; GA, gangliosides; MM-, monomethyl; PA, phosphatidic acid, PC, phosphatidylcholine; PCho, choline phosphate; PE, phosphatidylethanolamine; PEtn, ethanolamine phosphate; PG, phosphatidylglycerol; PI, phosphatidylinositol; PMT, phosphoethanolamine N-methyltransferase; PK, polyketides; PR, prenols; PS, phosphatidylserine; PSD, phosphatidylserine decarboxylase; PSS, phosphatidylserine synthase; SD, serine decarboxylase; SM, sphingomyelin; TG, triglyceride; TM-,trimethyl; *not detected.
(TIF)

S13 Fig. Peroxide-induced disruption of protein abundance for enzymes involved in the synthesis of phosphatidylcholine (PC) and phosphatidylethanolamine (PE) lipids within *P. falciparum* parasites. Values are the average fold change (± SD) relative to the untreated control of at least three biological replicates. Choline-phosphate cytidyltransferase (CCT) was only identified in one OZ439 experiment, therefore the mean from one experiment is shown. The last step in both the PC and PE branches of the Kennedy Pathways are catalysed by the enzyme choline/ethanolamine phosphotransferase (CEPT). For ease of representation, the abundance of CEPT is only shown for the PC branch of the pathway. * p-value < 0.05. CCT, choline-phosphate cytidyltransferase; CDP-, cytidine-diphospho-; CEPT, choline/ethanolamine phosphotransferase; Cer, ceramide; Cho, choline; CK, choline kinase; CMP, cytidine monophosphate; DAG/DG, diglyceride; DM-, dimethyl-; ECT, ethanolamine-phosphate cyitidyltransferase; EK, ethanolamine kinase; Etn, ethanolamine; GA, gangliosides; MM-, monomethyl; PA, phosphatidic acid, PC, phosphatidylcholine; PCho, choline phosphate; PE, phosphatidylethanolamine; PEtn, ethanolamine phosphate; PG, phosphatidylglycerol; PI, phosphatidylinositol; PMT, phosphoethanolamine N-methyltransferase; PK, polyketides; PR, prenols; PS, phosphatidylserine; PSD, phosphatidylserine decarboxylase; PSS, phosphatidylserine synthase; SD, serine decarboxylase; SM, sphingomyelin; TG, triglyceride; TM-,trimethyl.
(TIF)

S14 Fig. Time-dependent peroxide-induced perturbations of metabolites in the phosphatidylcholine (PC) and phosphatidylethanolamine *de novo* synthesis pathways in ring infected cultures. The abundances of each of the metabolites after treatment with OZ277 (blue), OZ439 (green) and DHA (red) are the average fold change (± SD) relative to the untreated control of four biological replicates. Metabolites in red were increased in abundance after drug treatment. Enzyme names are shown in solid boxes. The dashed arrow represents an alternative route for the synthesis of PC from ethanolamine (Etn) in *P. falciparum* parasites. CCT, choline-phosphate cytidyltransferase; CDP-, cytidine-diphospho-; CEPT, choline/ethanolamine phosphotransferase; Cho, choline; CK, choline kinase; CMP, cytidine monophosphate; ECT, ethanolamine-phosphate cytidyltransferase; EK, ethanolamine kinase; Etn, ethanolamine; PC, phosphatidylcholine; PE, phosphatidylethanolamine; PCho, choline phosphate; PEtn, ethanolamine phosphate; PMT, phosphoethanolamine N-methyltransferase; *not detected.
(TIF)

S15 Fig. Peroxide-induced perturbation of metabolites in the pyrimidine biosynthesis pathway in trophozoite-stage parasite cultures. Values are the average fold change (± SD) relative to the untreated control of three biological replicates. For the pyrimidine biosynthesis pathway, blue circles represent metabolites that are decreased in abundance, yellow circles represent no change and black circles represent metabolites that were not detected. Hb, haemoglobin; UMP, uridine monophosphate.
(TIF)

S16 Fig. Peroxide-induced disruption of protein abundance for enzymes involved in the *P. falciparum* pyrimidine biosynthesis pathway. Values are the average fold change (± SD) relative to the untreated control of at least three biological replicates. Orotate phosphoribosyltransferase was not detected in OZ277 treated parasites and was only identified in one OZ439 experiment. * p-value < 0.05.
(TIF)

S1 Dataset. IDEOM metabolomics output for OZ277, OZ439 and DHA treatment of P. falciparum (3D7 strain) ring and trophozoite infected RBC cultures and uninfected RBC cultures.
(XLSX)

S2 Dataset. IDEOM metabolomics output for OZ277, OZ439 and DHA treatment of Cam3.II^{R539T} (artemisinin resistant) and Cam3.II^{rev} (artemisinin sensitive) *P. falciparum* parasite lines.
(XLSX)

S3 Dataset. Peptidomics dataset for OZ277, OZ439 and DHA treatment (3 h) of *P. falciparum* trophozoite infected RBC cultures (3D7 strain).
(XLSX)

S4 Dataset. Peptidomics dataset for DHA treatment (1 h) of *P. falciparum* trophozoite infected RBC cultures (Cam3.II^{rev}, artemisinin sensitive).
(XLSX)

S5 Dataset. Proteomics dataset for OZ277, OZ439 and DHA treatment of *P. falciparum* trophozoite infected RBC cultures (3D7 strain).
(XLSX)

Acknowledgments

The authors thank Professor Matthew Bogyo (Stanford University School of Medicine) and Doctor Edgar Deu (The Francis Crick Institute) for providing the FY01 probe. Doctor Edgar Deu is also gratefully acknowledged for advice regarding activity-based protein profiling experiments. The authors thank Professor David Fidock (Columbia University) for provision of the genetically modified Cam3.II^{R539T} and Cam3.II^{rev} *P. falciparum* isolates. The Monash Proteomics and Metabolomics Facility (Parkville Node) provided technical assistance with metabolomics and proteomics experiments. The Australian Red Cross Blood Service in Melbourne donated human red blood cells for *in vitro* parasite cultivation.

Author Contributions

Conceptualization: Darren J. Creek.

Data curation: Ghizal Siddiqui, Darren J. Creek.

Formal analysis: Carlo Giannangelo, Ghizal Siddiqui.

Funding acquisition: Susan A. Charman, Darren J. Creek.

Investigation: Carlo Giannangelo, Ghizal Siddiqui, Amanda De Paoli.

Methodology: Carlo Giannangelo, Ghizal Siddiqui, Amanda De Paoli, Bethany M. Anderson, Laura E. Edgington-Mitchell.

Project administration: Darren J. Creek.

Resources: Laura E. Edgington-Mitchell, Darren J. Creek.

Software: Darren J. Creek.

Supervision: Ghizal Siddiqui, Laura E. Edgington-Mitchell, Susan A. Charman, Darren J. Creek.

Validation: Carlo Giannangelo.

Visualization: Carlo Giannangelo, Ghizal Siddiqui.

Writing – original draft: Carlo Giannangelo.

Writing – review & editing: Carlo Giannangelo, Ghizal Siddiqui, Laura E. Edgington-Mitchell, Susan A. Charman, Darren J. Creek.

References

1. WHO. World Malaria Report 2017. Geneva: World Health Organisation, 2017.
2. Enserink M. Malaria's drug miracle in danger. Science. 2010; 328: 844–6. https://doi.org/10.1126/science.328.5980.844 PMID: 20466917.
3. Meshnick SR, Thomas A, Ranz A, Xu CM, Pan HZ. Artemisinin (qinghaosu): the role of intracellular hemin in its mechanism of antimalarial action. Mol Biochem Parasitol. 1991; 49: 181–9. https://doi.org/10.1016/0166-6851(91)90062-b PMID: 1775162.
4. Meshnick SR, Yang YZ, Lima V, Kuypers F, Kamchonwongpaisan S, Yuthavong Y. Iron-dependent free radical generation from the antimalarial agent artemisinin (qinghaosu). Antimicrob Agents Chemother. 1993; 37: 1108–14. https://doi.org/10.1128/aac.37.5.1108 PMID: 8517699.
5. Posner GH, Oh CH. Regiospecifically oxygen-18 labeled 1, 2, 4-trioxane: a simple chemical model system to probe the mechanism (s) for the antimalarial activity of artemisinin (qinghaosu). J Am Chem Soc. 1992; 114: 8328–9. https://doi.org/10.1021/ja00047a076
6. Zhang F, Gosser DK, Meshnick SR. Hemin-catalyzed decomposition of artemisinin (qinghaosu). Biochem Pharmacol. 1992; 43: 1805–9. https://doi.org/10.1016/0006-2952(92)90713-s PMID: 1575774.
7. Woodrow CJ, Haynes RK, Krishna S. Artemisinins. Postgrad Med J. 2005; 81: 71–8. https://doi.org/10.1136/pgmj.2004.028399 PMID: 15701735; PubMed Central PMCID: PMC1743191.
8. Watsierah CA, Ouma C. Access to artemisinin-based combination therapy (ACT) and quinine in malaria holoendemic regions of western Kenya. Malar J. 2014; 13: 290. https://doi.org/10.1186/1475-2875-13-290 PMID: 25066600.
9. Wells TNC, van Huijsduijnen RH, Van Voorhis WC. Malaria medicines: a glass half full? Nat Rev Drug Discov. 2015; 14: 424–42. https://doi.org/10.1038/nrd4573 PMID: 26000721
10. Dondorp AM, Nosten F, Yi P, Das D, Phyo AP, Tarning J, et al. Artemisinin resistance in *Plasmodium falciparum* malaria. N Engl J Med. 2009; 361: 455–67. https://doi.org/10.1056/NEJMoa0808859 PMID: 19641202; PubMed Central PMCID: PMC3495232.
11. Vennerstrom JL, Arbe-Barnes S, Brun R, Charman SA, Chiu FC, Chollet J, et al. Identification of an antimalarial synthetic trioxolane drug development candidate. Nature. 2004; 430: 900–4. https://doi.org/10.1038/nature02779 PMID: 15318224.
12. Gautam A, Ahmed T, Sharma P, Varshney B, Kothari M, Saha N, et al. Pharmacokinetics and pharmacodynamics of arterolane maleate following multiple oral doses in adult patients with *P. falciparum* malaria. J Clin Pharmacol. 2011; 51: 1519–28. https://doi.org/10.1177/0091270010385578 PMID: 21148048.

13. Saha N, Moehrle JJ, Zutshi A, Sharma P, Kaur P, Iyer SS. Safety, tolerability and pharmacokinetic profile of single and multiple oral doses of arterolane (RBx11160) maleate in healthy subjects. J Clin Pharmacol. 2014; 54: 386–93. https://doi.org/10.1002/jcph.232 PMID: 24242999.

14. Zhou L, Alker A, Ruf A, Wang X, Chiu FC, Morizzi J, et al. Characterization of the two major CYP450 metabolites of ozonide (1, 2, 4-trioxolane) OZ277. Bioorg Med Chem Lett. 2008; 18: 1555–8. https://doi.org/10.1016/j.bmcl.2008.01.087 PMID: 18262417

15. Charman SA, Arbe-Barnes S, Bathurst IC, Brun R, Campbell M, Charman WN, et al. Synthetic ozonide drug candidate OZ439 offers new hope for a single-dose cure of uncomplicated malaria. Proc Natl Acad Sci U S A. 2011; 108: 4400–5. Epub 2011/02/09. https://doi.org/10.1073/pnas.1015762108 PMID: 21300861.

16. Moehrle JJ, Duparc S, Siethoff C, van Giersbergen PL, Craft JC, Arbe-Barnes S, et al. First-in-man safety and pharmacokinetics of synthetic ozonide OZ439 demonstrates an improved exposure profile relative to other peroxide antimalarials. Br J Clin Pharmacol. 2013; 75: 524–37. https://doi.org/10.1111/j.1365-2125.2012.04368.x PMID: 22759078.

17. Phyo AP, Jittamala P, Nosten FH, Pukrittayakamee S, Imwong M, White NJ, et al. Antimalarial activity of artefenomel (OZ439), a novel synthetic antimalarial endoperoxide, in patients with *Plasmodium falciparum* and *Plasmodium vivax* malaria: an open-label phase 2 trial. Lancet Infect Dis. 2016; 16: 61–9. https://doi.org/10.1016/S1473-3099(15)00320-5 PMID: 26448141.

18. McCarthy JS, Baker M, O'Rourke P, Marquart L, Griffin P, van Huijsduijnen RH, et al. Efficacy of OZ439 (artefenomel) against early *Plasmodium falciparum* blood-stage malaria infection in healthy volunteers. J Antimicrob Chemother. 2016; 71: 2620–7. https://doi.org/10.1093/jac/dkw174 PMID: 27272721.

19. Wang J, Zhang C-J, Chia WN, Loh CC, Li Z, Lee YM, et al. Haem-activated promiscuous targeting of artemisinin in *Plasmodium falciparum*. Nat Commun. 2015; 6: 10111. https://doi.org/10.1038/ncomms10111 PMID: 26694030

20. Ismail HM, Barton V, Phanchana M, Charoensutthivarakul S, Wong MHL, Hemingway J, et al. Artemisinin activity-based probes identify multiple molecular targets within the asexual stage of the malaria parasites *Plasmodium falciparum* 3D7. Proc Natl Acad Sci U S A. 2016; 113: 2080–5. https://doi.org/10.1073/pnas.1600459113 PMID: 26858419.

21. Bridgford JL, Xie SC, Cobbold SA, Pasaje CFA, Herrmann S, Yang T, et al. Artemisinin kills malaria parasites by damaging proteins and inhibiting the proteasome. Nat Commun. 2018; 9: 3801. https://doi.org/10.1038/s41467-018-06221-1 PMID: 30228310.

22. Tilley L, Straimer J, Gnädig NF, Ralph SA, Fidock DA. Artemisinin action and resistance in *Plasmodium falciparum*. Trends Parasitol. 2016; 32: 682–96. https://doi.org/10.1016/j.pt.2016.05.010 PMID: 27289273.

23. Bhattacharjee S, Coppens I, Mbengue A, Suresh N, Ghorbal M, Slouka Z, et al. Remodeling of the malaria parasite and host human red cell by vesicle amplification that induces artemisinin resistance. Blood. 2018; 131: 1234–47. https://doi.org/10.1182/blood-2017-11-814665 PMID: 29363540

24. Mbengue A, Bhattacharjee S, Pandharkar T, Liu HN, Estiu G, Stahelin RV, et al. A molecular mechanism of artemisinin resistance in *Plasmodium falciparum* malaria. Nature. 2015; 520: 683–7. https://doi.org/10.1038/nature14412 WOS:000353689700051. PMID: 25874676

25. Tang Y, Dong Y, Wang X, Sriraghavan K, Wood JK, Vennerstrom JL. Dispiro-1,2,4-trioxane analogues of a prototype dispiro-1,2,4-trioxolane: mechanistic comparators for artemisinin in the context of reaction pathways with iron(II). J Org Chem. 2005; 70: 5103–10. https://doi.org/10.1021/jo050385+ PMID: 15960511.

26. Jourdan J, Matile H, Reift E, Biehlmaier O, Dong Y, Wang X, et al. Monoclonal antibodies that recognize the alkylation signature of antimalarial ozonides OZ277 (arterolane) and OZ439 (artefenomel). ACS Infect Dis. 2015; 2: 54–61. https://doi.org/10.1021/acsinfecdis.5b00090 PMID: 26819968

27. Ismail HM, Barton VE, Panchana M, Charoensutthivarakul S, Biagini GA, Ward SA, et al. A click chemistry-based proteomic approach reveals that 1, 2, 4-trioxolane and artemisinin antimalarials share a common protein alkylation profile. Angewandte Chemie International Ed In English. 2016; 55: 6401–5.

28. Giannangelo C, Stingelin L, Yang T, Tilley L, Charman SA, Creek DJ. Parasite-mediated degradation of synthetic ozonide antimalarials impacts *in vitro* antimalarial activity. Antimicrob Agents Chemother. 2018; 62: e01566–17. https://doi.org/10.1128/AAC.01566-17 PMID: 29263074.

29. Valecha N, Krudsood S, Tangpukdee N, Mohanty S, Sharma S, Tyagi P, et al. Arterolane maleate plus piperaquine phosphate for treatment of uncomplicated *Plasmodium falciparum* malaria: a comparative, multicenter, randomized clinical trial. Clin Infect Dis. 2012; 55: 663–71. https://doi.org/10.1093/cid/cis475 PMID: 22586253

30. Yang T, Xie SC, Cao P, Giannangelo C, McCaw J, Creek DJ, et al. Comparison of the exposure time-dependence of the activities of synthetic ozonide antimalarials and dihydroartemisinin against K13

wild-type and mutant *Plasmodium falciparum* strains. Antimicrob Agents Chemother. 2016; 60: 4501–10. https://doi.org/10.1128/AAC.00574-16 PMID: 27161632.

31. Straimer J, Gnadig NF, Witkowski B, Amaratunga C, Duru V, Ramadani AP, et al. Drug resistance. K13-propeller mutations confer artemisinin resistance in *Plasmodium falciparum* clinical isolates. Science. 2015; 347: 428–31. https://doi.org/10.1126/science.1260867 PMID: 25502314.

32. Dogovski C, Xie SC, Burgio G, Bridgford J, Mok S, McCaw JM, et al. Targeting the cell stress response of *Plasmodium falciparum* to overcome artemisinin resistance. PLoS Biol. 2015; 13: e1002132. https://doi.org/10.1371/journal.pbio.1002132 PMID: 25901609.

33. Rosenthal PJ. Falcipain cysteine proteases of malaria parasites: An update. Biochim Biophys Acta Proteins Proteom. 2020; 1868: 140362. https://doi.org/10.1016/j.bbapap.2020.140362 PMID: 31927030.

34. Sijwali PS, Rosenthal PJ. Gene disruption confirms a critical role for the cysteine protease falcipain-2 in hemoglobin hydrolysis by *Plasmodium falciparum*. Proc Natl Acad Sci U S A. 2004; 101: 4384–9. https://doi.org/10.1073/pnas.0307720101 PMID: 15070727; PubMed Central PMCID: PMC384756.

35. Combrinck JM, Fong KY, Gibhard L, Smith PJ, Wright DW, Egan TJ. Optimization of a multi-well colorimetric assay to determine haem species in *Plasmodium falciparum* in the presence of anti-malarials. Malar J. 2015; 14: 253. Epub 2015/06/24. https://doi.org/10.1186/s12936-015-0729-9 PMID: 26099266; PubMed Central PMCID: PMC4484700.

36. Goldberg DE. Hemoglobin degradation. In: Compans RW, Cooper MD, Honjo T, Koprowski H, Melchers F, Oldstone MBA, et al., editors. Malaria: Drugs, disease and post-genomic biology. Current Topics in Microbiology and Immunology. 295: Springer Berlin Heidelberg; 2005. p. 275–91.

37. Siddiqui G, Srivastava A, Russell AS, Creek DJ. Multi-omics based identification of specific biochemical changes associated with PfKelch13-mutant artemisinin resistant *Plasmodium falciparum*. J Infect Dis. 2017; 215: 1435–44. Epub 2017/04/04. https://doi.org/10.1093/infdis/jix156 PMID: 28368494.

38. Klemba M, Gluzman I, Goldberg DE. A *Plasmodium falciparum* dipeptidyl aminopeptidase I participates in vacuolar hemoglobin degradation. J Biol Chem. 2004; 279: 43000–7. https://doi.org/10.1074/jbc.M408123200 PMID: 15304495.

39. McGowan S. Working in concert: the metalloaminopeptidases from *Plasmodium falciparum*. Curr Opin Struct Biol. 2013; 23: 828–35. https://doi.org/10.1016/j.sbi.2013.07.015 PMID: 23948130.

40. Sanman LE, Bogyo M. Activity-based profiling of proteases. Annu Rev Biochem. 2014; 83: 249–73. https://doi.org/10.1146/annurev-biochem-060713-035352 PMID: 24905783.

41. Greenbaum DC, Baruch A, Grainger M, Bozdech Z, Medzihradszky KF, Engel J, et al. A role for the protease falcipain 1 in host cell invasion by the human malaria parasite. Science. 2002; 298: 2002–6. https://doi.org/10.1126/science.1077426 PMID: 12471262.

42. Deu E, Leyva MJ, Albrow VE, Rice MJ, Ellman JA, Bogyo M. Functional studies of *Plasmodium falciparum* dipeptidyl aminopeptidase I using small molecule inhibitors and active site probes. Chem Biol. 2010; 17: 808–19. https://doi.org/10.1016/j.chembiol.2010.06.007 PMID: 20797610.

43. Liu J, Istvan ES, Gluzman IY, Gross J, Goldberg DE. *Plasmodium falciparum* ensures its amino acid supply with multiple acquisition pathways and redundant proteolytic enzyme systems. Proc Natl Acad Sci U S A. 2006; 103: 8840–5. https://doi.org/10.1073/pnas.0601876103 PMID: 16731623; PubMed Central PMCID: PMC1470969.

44. Olliaro P. Mode of action and mechanisms of resistance for antimalarial drugs. Pharmacol Ther. 2001; 89: 207–19. https://doi.org/10.1016/s0163-7258(00)00115-7 PMID: 11316521.

45. Cobbold SA, Chua HH, Nijagal B, Creek DJ, Ralph SA, McConville MJ. Metabolic dysregulation induced in *Plasmodium falciparum* by dihydroartemisinin and other front line antimalarial drugs. J Infect Dis. 2015; 213: 276–86. https://doi.org/10.1093/infdis/jiv372 PMID: 26150544.

46. Creek DJ, Chua HH, Cobbold SA, Nijagal B, MacRae JI, Dickerman BK, et al. Metabolomics-based screening of the malaria box reveals both novel and established mechanisms of action. Antimicrob Agents Chemother. 2016; 60: 6650–63. https://doi.org/10.1128/AAC.01226-16 PMID: 27572396.

47. Allman EL, Painter HJ, Samra J, Carrasquilla M, Llinás M. Metabolomic profiling of the malaria box reveals antimalarial target pathways. Antimicrob Agents Chemother. 2016; 60: 6635–49. https://doi.org/10.1128/AAC.01224-16 PMID: 27572391.

48. Sherman IW, Tanigoshi L. Incorporation of 14 C-amino-acids by malaria (*Plasmodium lophurae*) IV. *In vivo* utilization of host cell haemoglobin. Int J Biochem. 1970; 1: 635–7. https://doi.org/10.1016/0020-711X(70)90033-9

49. Lew VL, Tiffert T, Ginsburg H. Excess hemoglobin digestion and the osmotic stability of *Plasmodium falciparum*–infected red blood cells. Blood. 2003; 101: 4189–94. https://doi.org/10.1182/blood-2002-08-2654 PMID: 12531811.

50. Krugliak M, Zhang J, Ginsburg H. Intraerythrocytic *Plasmodium falciparum* utilizes only a fraction of the amino acids derived from the digestion of host cell cytosol for the biosynthesis of its proteins. Mol Biochem Parasitol. 2002; 119: 249–56. https://doi.org/10.1016/s0166-6851(01)00427-3 PMID: 11814576.

51. Francis SE, Sullivan DJ Jr, Goldberg, E D. Hemoglobin metabolism in the malaria parasite *Plasmodium falciparum*. Annu Rev Microbiol. 1997; 51: 97–123. https://doi.org/10.1146/annurev.micro.51.1.97 PMID: 9343345.

52. Klonis N, Crespo-Ortiz MP, Bottova I, Abu-Bakar N, Kenny S, Rosenthal PJ, et al. Artemisinin activity against *Plasmodium falciparum* requires hemoglobin uptake and digestion. Proc Natl Acad Sci U S A. 2011; 108: 11405–10. https://doi.org/10.1073/pnas.1104063108 PMID: 21709259.

53. Gruring C, Spielmann T. Imaging of live malaria blood stage parasites. Methods Enzymol. 2012; 506: 81–92. https://doi.org/10.1016/B978-0-12-391856-7.00029-9 PMID: 22341220.

54. Orjih AU, Fitch CD. Hemozoin production by *Plasmodium falciparum*: variation with strain and exposure to chloroquine. Biochim Biophys Acta Gen Subj. 1993; 1157: 270–4. https://doi.org/10.1016/0304-4165(93)90109-l PMID: 8323956.

55. Abu Bakar N, Klonis N, Hanssen E, Chan C, Tilley L. Digestive-vacuole genesis and endocytic processes in the early intraerythrocytic stages of *Plasmodium falciparum*. J Cell Sci. 2010; 123: 441–50. Epub 2010/01/14. https://doi.org/10.1242/jcs.061499 PMID: 20067995.

56. Ponpuak M, Klemba M, Park M, Gluzman IY, Lamppa GK, Goldberg DE. A role for falcilysin in transit peptide degradation in the *Plasmodium falciparum* apicoplast. Mol Microbiol. 2007; 63: 314–34. https://doi.org/10.1111/j.1365-2958.2006.05443.x PMID: 17074076.

57. Murata CE, Goldberg DE. *Plasmodium falciparum* falcilysin: a metalloprotease with dual specificity. J Biol Chem. 2003; 278: 38022–8. https://doi.org/10.1074/jbc.M306842200 PMID: 12876284.

58. Giannangelo C, Fowkes FJI, Simpson JA, Charman SA, Creek DJ. Ozonide antimalarial activity in the context of artemisinin-resistant malaria. Trends Parasitol. 2019. https://doi.org/10.1016/j.pt.2019.05.002 PMID: 31176584

59. Xie SC, Dogovski C, Hanssen E, Chiu F, Yang T, Crespo MP, et al. Haemoglobin degradation underpins the sensitivity of early ring stage *Plasmodium falciparum* to artemisinins. J Cell Sci. 2016; 129: 406–16. https://doi.org/10.1242/jcs.178830 PMID: 26675237.

60. Straimer J, Gnädig NF, Stokes BH, Ehrenberger M, Crane AA, Fidock DA. *Plasmodium falciparum* K13 mutations differentially impact ozonide susceptibility and parasite fitness in vitro. mBio. 2017; 8: e00172–17. https://doi.org/10.1128/mBio.00172-17 PMID: 28400526.

61. Baumgärtner F, Jourdan J, Scheurer C, Blasco B, Campo B, Mäser P, et al. *In vitro* activity of antimalarial ozonides against an artemisinin-resistant isolate. Malar J. 2017; 16: 45. https://doi.org/10.1186/s12936-017-1696-0 PMID: 28122617

62. Siriwardana A, Iyengar K, Roepe PD. Endoperoxide drug cross-resistance patterns for *Plasmodium falciparum* exhibiting an artemisinin delayed-clearance phenotype. Antimicrob Agents Chemother. 2016; 60: 6952–6. https://doi.org/10.1128/AAC.00857-16 PMID: 27600038

63. Yang T, Yeoh LM, Tutor MV, Dixon MW, McMillan PJ, Xie SC, et al. Decreased K13 abundance reduces hemoglobin catabolism and proteotoxic stress, underpinning artemisinin resistance. Cell Rep. 2019; 29: 2917–28.e5. https://doi.org/10.1016/j.celrep.2019.10.095 PMID: 31775055

64. Birnbaum J, Scharf S, Schmidt S, Jonscher E, Hoeijmakers WAM, Flemming S, et al. A Kelch13-defined endocytosis pathway mediates artemisinin resistance in malaria parasites. Science. 2020; 367: 51–9. Epub 2020/01/04. https://doi.org/10.1126/science.aax4735 PMID: 31896710.

65. Rocamora F, Zhu L, Liong KY, Dondorp A, Miotto O, Mok S, et al. Oxidative stress and protein damage responses mediate artemisinin resistance in malaria parasites. PLoS Pathog. 2018; 14: e1006930. https://doi.org/10.1371/journal.ppat.1006930 PMID: 29538461.

66. Phompradit P, Chaijaroenkul W, Na-Bangchang K. Cellular mechanisms of action and resistance of *Plasmodium falciparum* to artemisinin. Parasitol Res. 2017; 116: 3331–9. https://doi.org/10.1007/s00436-017-5647-z PMID: 29127525.

67. del Pilar Crespo M, Avery TD, Hanssen E, Fox E, Robinson TV, Valente P, et al. Artemisinin and a series of novel endoperoxide antimalarials exert early effects on digestive vacuole morphology. Antimicrob Agents Chemother. 2008; 52: 98–109. https://doi.org/10.1128/AAC.00609-07 PMID: 17938190.

68. Maeno Y, Toyoshima T, Fujioka H, Ito Y, Meshnick SR, Benakis A, et al. Morphologic effects of artemisinin in *Plasmodium falciparum*. Am J Trop Med Hyg. 1993; 49: 485–91. Epub 1993/10/01. https://doi.org/10.4269/ajtmh.1993.49.485 PMID: 8214279.

69. O'Neill PM, Posner GH. A medicinal chemistry perspective on artemisinin and related endoperoxides. J Med Chem. 2004; 47: 2945–64. https://doi.org/10.1021/jm030571c PMID: 15163175.

70. Hartwig CL, Lauterwasser EMW, Mahajan SS, Hoke JM, Cooper RA, Renslo AR. Investigating the antimalarial action of 1,2,4-trioxolanes with fluorescent chemical probes. J Med Chem. 2011; 54: 8207–13. https://doi.org/10.1021/jm2012003 PMID: 22023506.

71. Hartwig CL, Rosenthal AS, D'Angelo J, Griffin CE, Posner GH, Cooper RA. Accumulation of artemisinin trioxane derivatives within neutral lipids of *Plasmodium falciparum* malaria parasites is endoperoxide-dependent. Biochem Pharmacol. 2009; 77: 322–36. https://doi.org/10.1016/j.bcp.2008.10.015 PMID: 19022224.

72. Berman PA, Adams PA. Artemisinin enhances heme-catalysed oxidation of lipid membranes. Free Radical Biol Med. 1997; 22: 1283–8. https://doi.org/10.1016/S0891-5849(96)00508-4 PMID: 9098103.

73. Serran-Aguilera L, Denton H, Rubio-Ruiz B, Lopez-Gutierrez B, Entrena A, Izquierdo L, et al. *Plasmodium falciparum* Choline Kinase Inhibition Leads to a Major Decrease in Phosphatidylethanolamine Causing Parasite Death. Sci Rep. 2016; 6: 33189. Epub 2016/09/13. https://doi.org/10.1038/srep33189 PMID: 27616047; PubMed Central PMCID: PMC5018819.

74. Gulati S, Ekland EH, Ruggles KV, Chan RB, Jayabalasingham B, Zhou B, et al. Profiling the essential nature of lipid metabolism in asexual blood and gametocyte stages of *Plasmodium falciparum*. Cell Host Microbe. 2015; 18: 371–81. https://doi.org/10.1016/j.chom.2015.08.003 PMID: 26355219.

75. Vielemeyer O, McIntosh MT, Joiner KA, Coppens I. Neutral lipid synthesis and storage in the intraerythrocytic stages of *Plasmodium falciparum*. Mol Biochem Parasitol. 2004; 135: 197–209. https://doi.org/10.1016/j.molbiopara.2003.08.017 PMID: 15110461.

76. Hoang AN, Sandlin RD, Omar A, Egan TJ, Wright DW. The neutral lipid composition present in the digestive vacuole of *Plasmodium falciparum* concentrates heme and mediates β-hematin formation with an unusually low activation energy. Biochemistry. 2010; 49: 10107–16. https://doi.org/10.1021/bi101397u PMID: 20979358.

77. Jackson KE, Klonis N, Ferguson DJ, Adisa A, Dogovski C, Tilley L. Food vacuole-associated lipid bodies and heterogeneous lipid environments in the malaria parasite, *Plasmodium falciparum*. Mol Microbiol. 2004; 54: 109–22. https://doi.org/10.1111/j.1365-2958.2004.04284.x PMID: 15458409.

78. Pisciotta JM, Coppens I, Tripathi AK, Scholl PF, Shuman J, Bajad S, et al. The role of neutral lipid nanospheres in *Plasmodium falciparum* haem crystallization. Biochem J. 2007; 402: 197–204. https://doi.org/10.1042/BJ20060986 PMID: 17044814; PubMed Central PMCID: PMC1783988.

79. Fry M, Pudney M. Site of action of the antimalarial hydroxynaphthoquinone, 2-[*trans*-4-(4'-chlorophenyl) cyclohexyl]-3-hydroxy-1,4-naphthoquinone (566C80). Biochem Pharmacol. 1992; 43: 1545–53. https://doi.org/10.1016/0006-2952(92)90213-3 PMID: 1314606.

80. Birrell GW, Challis MP, De Paoli A, Anderson D, Devine SM, Heffernan GD, et al. Multi-omic characterisation of the mode of action of a potent new antimalarial compound, JPC-3210, against *Plasmodium falciparum*. Mol Cell Proteomics. 2019. Epub 2019/12/15. https://doi.org/10.1074/mcp.RA119.001797 PMID: 31836637.

81. Zhang M, Gallego-Delgado J, Fernandez-Arias C, Waters NC, Rodriguez A, Tsuji M, et al. Inhibiting the *Plasmodium* eIF2α kinase PK4 prevents artemisinin-induced latency. Cell Host Microbe. 2017; 22: 766–76.e4. https://doi.org/10.1016/j.chom.2017.11.005 PMID: 29241041.

82. Wek RC, Jiang H-Y, Anthony TG. Coping with stress: eIF2 kinases and translational control. Biochem Soc Trans. 2006; 34: 7–11. https://doi.org/10.1042/BST20060007 PMID: 16246168.

83. Paloque L, Ramadani AP, Mercereau-Puijalon O, Augereau J-M, Benoit-Vical F. *Plasmodium falciparum*: multifaceted resistance to artemisinins. Malar J. 2016; 15: 149. https://doi.org/10.1186/s12936-016-1206-9 PMID: 26955948

84. Ponts N, Saraf A, Chung D-WD, Harris A, Prudhomme J, Washburn MP, et al. Unraveling the ubiquitome of the human malaria parasite. J Biol Chem. 2011; 286: 40320–30. https://doi.org/10.1074/jbc.M111.238790 PMID: 21930698.

85. Aminake MN, Arndt H-D, Pradel G. The proteasome of malaria parasites: A multi-stage drug target for chemotherapeutic intervention? Int J Parasitol Drugs Drug Resist. 2012; 2: 1–10. https://doi.org/10.1016/j.ijpddr.2011.12.001 PMID: 24533266

86. Macintyre F, Adoke Y, Tiono AB, Duong TT, Mombo-Ngoma G, Bouyou-Akotet M, et al. A randomised, double-blind clinical phase II trial of the efficacy, safety, tolerability and pharmacokinetics of a single dose combination treatment with artefenomel and piperaquine in adults and children with uncomplicated *Plasmodium falciparum* malaria. BMC Med. 2017; 15: 181. https://doi.org/10.1186/s12916-017-0940-3 PMID: 28988541.

87. Trager W, Jensen JB. Human malaria parasites in continuous culture. Science. 1976; 193: 673–5. https://doi.org/10.1126/science.781840 PMID: 781840.

88. Lambros C, Vanderberg JP. Synchronization of *Plasmodium falciparum* erythrocytic stages in culture. J Parasitol. 1979; 65: 418–20. PMID: 383936.

89. Giannangelo CR, Ellis KM, Sexton AE, Stoessel D, Creek DJ. The role of metabolomics in antiparasitic drug discovery. Comprehensive analysis of parasite biology: from metabolism to drug discovery. 7. Weinheim, Germany: Wiley-VCH; 2016. p. 321–42.

90. Creek DJ, Jankevics A, Burgess KE, Breitling R, Barrett MP. IDEOM: an Excel interface for analysis of LC-MS-based metabolomics data. Bioinformatics. 2012; 28: 1048–9. https://doi.org/10.1093/bioinformatics/bts069 PMID: 22308147.

91. Sumner LW, Amberg A, Barrett D, Beale MH, Beger R, Daykin CA, et al. Proposed minimum reporting standards for chemical analysis. Metabolomics. 2007; 3: 211–21. https://doi.org/10.1007/s11306-007-0082-2 PMID: 24039616.

92. Creek DJ, Jankevics A, Breitling R, Watson DG, Barrett MP, Burgess KE. Toward global metabolomics analysis with hydrophilic interaction liquid chromatography-mass spectrometry: improved metabolite identification by retention time prediction. Anal Chem. 2011; 83: 8703–10. https://doi.org/10.1021/ac2021823 PMID: 21928819.

93. Xia J, Sinelnikov IV, Han B, Wishart DS. MetaboAnalyst 3.0—making metabolomics more meaningful. Nucleic Acids Res. 2015; 43: W251–W7. https://doi.org/10.1093/nar/gkv380 PMID: 25897128.

94. Rappsilber J, Ishihama Y, Mann M. Stop and go extraction tips for matrix-assisted laser desorption/ionization, nanoelectrospray, and LC/MS sample pretreatment in proteomics. Anal Chem. 2003; 75: 663–70. https://doi.org/10.1021/ac026117i PMID: 12585499

95. Zhang J, Xin L, Shan B, Chen W, Xie M, Yuen D, et al. PEAKS DB: de novo sequencing assisted database search for sensitive and accurate peptide identification. Mol Cell Proteomics. 2012; 11: M111.010587. https://doi.org/10.1074/mcp.M111.010587 PMID: 22186715.

96. Boersema PJ, Raijmakers R, Lemeer S, Mohammed S, Heck AJ. Multiplex peptide stable isotope dimethyl labeling for quantitative proteomics. Nat Protoc. 2009; 4: 484–94. https://doi.org/10.1038/nprot.2009.21 PMID: 19300442.

97. Lin Y, Liu Y, Li J, Zhao Y, He Q, Han W, et al. Evaluation and optimization of removal of an acid-insoluble surfactant for shotgun analysis of membrane proteome. Electrophoresis. 2010; 31: 2705–13. https://doi.org/10.1002/elps.201000161 PMID: 20665523.

98. Cox J, Mann M. MaxQuant enables high peptide identification rates, individualized ppb-range mass accuracies and proteome-wide protein quantification. Nat Biotechnol. 2008; 26: 1367–72. https://doi.org/10.1038/nbt.1511 PMID: 19029910.

99. Dallas DC, Guerrero A, Parker EA, Robinson RC, Gan J, German JB, et al. Current peptidomics: Applications, purification, identification, quantification, and functional analysis. Proteomics. 2015; 15: 1026–38. https://doi.org/10.1002/pmic.201400310 PMID: 25429922.

100. Szklarczyk D, Morris JH, Cook H, Kuhn M, Wyder S, Simonovic M, et al. The STRING database in 2017: quality-controlled protein–protein association networks, made broadly accessible. Nucleic Acids Res. 2016; 45: D362–D8. https://doi.org/10.1093/nar/gkw937 PMID: 27924014.

101. Shannon P, Markiel A, Ozier O, Baliga NS, Wang JT, Ramage D, et al. Cytoscape: A software environment for integrated models of biomolecular interaction networks. Genome Res. 2003; 13: 2498–504. https://doi.org/10.1101/gr.1239303 PMID: 14597658.

102. Edgington LE, Bogyo M. *In vivo* imaging and biochemical characterization of protease function using fluorescent activity-based probes. Curr Protoc Chem Biol. 2013; 5: 25–44. https://doi.org/10.1002/9780470559277.ch120235 PMID: 23788323.

103. Xie SC, Dogovski C, Kenny S, Tilley L, Klonis N. Optimal assay design for determining the *in vitro* sensitivity of ring stage *Plasmodium falciparum* to artemisinins. Int J Parasitol. 2014; 44: 893–9. https://doi.org/10.1016/j.ijpara.2014.07.008 PMID: 25161101

104. Perez-Riverol Y, Csordas A, Bai J, Bernal-Llinares M, Hewapathirana S, Kundu DJ, et al. The PRIDE database and related tools and resources in 2019: improving support for quantification data. Nucleic Acids Res. 2018; 47: D442–D50. https://doi.org/10.1093/nar/gky1106 PMID: 30395289